A Fundamental Study on the Relocation, Uptake, and Distribution of the Cs^+ Primary Ion Beam During the Secondary Ion Mass Spectrometry Analysis

Andrew John Giordani

Dissertation submitted to the faculty of the Virginia Polytechnic Institute and State University in partial fulfillment of the requirements for the degree of

Doctor of Philosophy

In

Materials Science and Engineering

Jerry L. Hunter Jr., Co-Chair
Louis J. Guido, Co-Chair
Carlos T.A. Suchicital
William T. Reynolds Jr.

March 10, 2016

Blacksburg, VA

Keywords: Secondary Ion Mass Spectrometry, Cs^+, MCs^+, Temperature, Cs Relocation

A Fundamental Study on the Relocation, Uptake, and Distribution of the Cs^+ Primary Ion Beam During the Secondary Ion Mass Spectrometry Analysis

Andrew John Giordani

Abstract

Combining cesium (Cs) bombardment with positive secondary molecular ion detection (MCs^+) can extend the analysis capability of Secondary Ion Mass Spectrometry (SIMS) from the dilute limit (<1%) to matrix elements. The MCs^+ technique has had great success in quantifying the sample composition of III-V semiconductors as well as dopants and/or impurities; however, it has been less effective at reducing the matrix effect for IV compounds, particularly Si-containing compounds, due to Cs overloading at the surface during the analysis from the Cs primary ion beam. The Cs overloading issue is attributable to the mobility and relocation of the implanted Cs to the surface; this effect happens almost instantaneously. Once the surface is overloaded with Cs, the excess Cs begins to reneutralize the ionization Cs and, as a result, the MCs^+ technique is ineffective at reducing the matrix effect.

This research provides new insights for improving the MCs^+ technique and elucidating the Cs mobility. A combination of multiple experimental techniques and theoretical modeling was implemented to assess the Cs retention, up-take, and distribution differences between group III-V and IV materials. Early experiments revealed a temperature-dependent component of the Cs mobility, prompting an investigation of this

phenomenon. Therefore, we designed, built, and installed a variable temperature stage for our SIMS with temperatures ranging from -150 to 300 °C. This enabled us to study the temperature-dependent component of the Cs mobility and the effect it has on the secondary ion emission processes. Additionally, a method was devised to quantify the amount of neutralization and ionization due to the relocated Cs. The results allow for a more thorough understanding of the material dependence on the Cs^+-sample interaction and the temperature component of the Cs mobility.

Dedication

To my grandfather, Pop G.

"Around here, however, we don't look backwards for very long. We keep moving forward, opening up new doors and doing new things… and curiosity keeps leading us down new paths."

–Walt Disney

"Success is never owned; it is only rented – and the rent is due everyday."

–Rory Vaden

Acknowledgements

Pursuing a PhD is like riding a roller coaster in the front seat with your hands up. During the ride, there are many mountains, valleys, and of course, a few corkscrews, but the key is to hold on and enjoy the ride!

I would like to thank Jerry Hunter, my advisor and friend, who taught me materials characterization in the spring of 2011. I am forever grateful for his class because it exposed me to scientific instruments that I had never seen or heard of before. This is where I found a passion and interest for instrument/technique development. None of this work would have been possible without Jerry's constant assistance, support, and advice. Jerry, I cannot put into words how thankful I am for everything that you have taught me and the opportunities that you have provided me.

I would also like to thank all the members of the NCFL for their invaluable assistance and support during my graduate studies. In particular, I would like thank Susette Sowers, Chris Winkler, Steve McCartney, and Bill Reynolds for providing words of encouragement and listening to my numerous struggles. I could not have asked for a better place to work for my assistantship. Most of all, I would like to thank my loving wife, Samantha, family, and friends for all their love and support during my graduate studies. A special thanks to my sister-in-law, Rachel Logan (editor in chief) for all the paper editing, it really meant a lot to me. Lastly, I would like to thank the Institute for Critical Technology and Applied Science and the Nanoscale Characterization and Fabrication Laboratory at Virginia Tech for their financial support for this work.

Table of Contents

Abstract ii

Dedication iv

Acknowledgements v

List of Figures x

List of Tables xiii

Attributions xiv

1. Introduction 1

1.1. Dissertation structure and organization 1

1.2. Significance and motivation 2

References 5

2. On the Evolution of Cs Droplets in SIMS Craters 5

2.1 Abstract 5

2.2 Authors and affiliations 6

2.3 Introduction 6

2.4 Experimental 7

2.5 Results and discussion 8

2.5.1 Atmospheric evolution of Cs droplets 8

2.5.2 O_2 evolution of Cs droplets 11

2.5.3 The effect of heat on Cs droplets 12

2.6 Conclusion 14

2.7 Acknowledgements 14

References 15

3. Temperature Dependent Relocation of the Cesium Primary Ion Beam During SIMS Analysis 15

3.1 Authors and affiliations 16

3.2 Abstract 16

3.3 Introduction 17

3.4 Experimental 18

3.5 Results and discussion 20

3.5.1 Behavior of Cs 20

3.5.2 Measuring Cs concentration 21

3.5.3 The effect of heat of Cs concentration 22

3.5.4 Effect of heat on Cs^+ ion yield 24

3.6 Conclusion 26

3.7 Acknowledgements 27

References 27

4. Design and Implementation of a Custom Built Variable Temperature Stage for a Secondary Ion Mass Spectrometer 28

4.1 Authors and affiliations 28

4.2 Abstract 29

4.3 Introduction 29

4.4 Design requirements 30

4.5 Design and implementation 31

4.5.1 Stage components 32

4.5.2 Stage electronics ... 35

4.5.3 Sample holder ... 37

4.5.4 Operation ... 38

4.6 Applications ... 40

4.6.1 Quickly achieving low background levels of atmospherics in Si ... 40

4.6.2 Reduced metastable decay of niobium hydrides ... 42

4.7 Summary and conclusions ... 45

4.8 Acknowledgements ... 45

References ... 45

5. Temperature Dependent Cs Retention, Distribution, and Ion Yield Changes During Cs^+ Bombardment SIMS ... 47

5.1 Authors and affiliations ... 47

5.2 Abstract ... 47

5.3 Introduction ... 49

5.4 Experimental ... 51

5.4.1 Materials ... 51

5.4.2 Heat-treatment XPS ... 52

5.4.3 Heat-treatment MEIS ... 52

5.4.4 SIMS: cesium build-up curves and sputter yields ... 53

5.5 Modeling and Cs ionization calculation ... 54

5.5.1 Modeling Cs retention: rapid relocation model ... 54

5.5.2 Calculation Cs ionization and neutralization ... 55

5.6 Results and discussion ... 57

5.6.1 *Ex situ* temperature-dependent Cs relocation and distribution 57

5.6.2 *In situ* temperature-dependent Cs 62

5.7 Summary and conclusions.. 72

5.8 Acknowledgments.. 73

References 74

6. Summary and Conclusions 75

Appendix: Copyright Permission Letters.. 78

List of Figures

Chapter 2

Figure 1: Evolution of Cs droplets as a function of atmospheric exposure; a: 4 min; b: 8 min; c: 18 min; d: 25 min; e: 60 min; f: 18 h. 10

Figure 2: EDS spectrum of the CsLα (4.29 keV) and CsLβ (4.62 keV) from the Cs droplet in Fig. 1a, confirming the presence of Cs in the droplet. 10

Figure 3: Evolution of Cs droplets with increasing O_2 exposure; a: 2 h; b: 2.5 h; c: 3 h; d: 4 h. 12

Figure 4: Effect of sample heating on Cs droplets; a: 4 h of atmospheric exposure – no heat; b: 4 h of atmospheric exposure followed by 250 °C for 1 h. 14

Chapter 3

Figure 1: XPS measured [Cs] as a function of temperature on InAs and Si. Illustrating the effect sample heating has on the implanted Cs and difference in retained Cs between InAs and Si. The effect that NEG (*in situ*) heating has on the distribution of the implanted Cs in InAs is also shown. 24

Figure 2: SIMS build up curve for InAs under regular and 640 $\mu A/cm^2$ NEG heated Cs^+ primary ion bombardment. 26

Chapter 4

Figure 1: (Color online) (a) Variable temperature stage assembled with main chamber door open. (b) Bottom view to show connections. 32

Figure 2: (Color online) (a) External vacuum connections for the variable temperature stage. (b) Internal electrical and liquid connections –view with the turbo pump removed, looking up at the bottom the variable temperature stage. 35

Figure 3: (Color online) Electronics for the variable temperature stage. 36

Figure 4: (Color online) Variable temperature sample holder. (a) Back of sample holder with Cu blocks not inserted. (b) Back of sample holder with Cu blocks inserted. (c) Assembled sample holder. 38

Figure 5: (Color online) Sample heating and cooling curves. Heating curve (squares) with 25 W output power. Cooling curve (circles) with chilled nitrogen gas (9.5 l/min flow rate) to -30 °C then switched to liquid nitrogen. 40

Figure 6: Nb mass spectra showing the difference in metastable decay between (a) room temperature (26 °C) and (b) -150 °C analysis temperatures. 44

Chapter 5

Figure 1: (Color online) XPS measured Cs concentration as a function of temperature on Si, Ge, SiC, InAs, GaAs, and GaSb. Illustrating the effect sample heating has on the mobility of the implanted Cs between group III-V and IV samples. 58

Figure 2: (Color online) Room temperature (RT) and heat-treatment MEIS spectra of GaAs and Ge after steady state Cs^+ bombardment. The GaAs RT and heat-treatment MEIS spectra were offset by 100, and the data density was reduced by 4x for all spectra for clarity. 61

Figure 3: (Color online) Variable temperture Cs^+-cesium build curves [(a)-(e)] demonstrating the Cs ionization dependence on Cs fluence and temperature. Data density was reduced for clarity. RT is room temperature. 65

List of Tables

Chapter 4

Table 1: SIMS atmospheric analysis comparison of traditional versus heating method. .42

Chapter 5

Table 1: Summary of the SY, Ψ_{rlc}, SY_{eff}, R_{21} (Cs_2^+/Cs^+), and steady state Cs ionization as function of temperature for Si, SiC, Ge, GaAs, and InAs. SIMS atmospheric analysis comparison of traditional versus heating method. RT is room temperature. 68

Attributions

Jerry Hunter – Ph.D., University of North Carolina, Chapel Hill, North Carolina, 1991. Director of Facilities at the Material Science Center, University of Wisconsin-Madison. Dissertation advisor and committee chair.

Christopher Winkler – Ph.D., Drexel University, Philadelphia, Pennsylvania, 2014. Senior Research Associate, Nanoscale Characterization and Fabrication Laboratory, Virginia Tech.

Jay Tuggle – Ph.D. student in the Materials Science and Engineering department at Virginia Tech.

Can Xu – Ph.D. student in the department of Physics and Astronomy at Rutgers, The State University of New Jersey.

Hang Dong Lee – Ph.D., University of Houston, Houston, Texas, 2006. Post-doctoral student in the department of Physics and Astronomy at Rutgers, The State University of New Jersey.

Torgny Gustafsson – Ph.D., Chalmers University of Technology, Sweden, 1973. Professor in the department of Physics and Astronomy at Rutgers, The State University of New Jersey.

Specific contributions from the co-authors of the publications in this dissertation.

Chapter 2

Mr. Tuggle and Dr. Winkler assisted with the Secondary Electron Microscope (SEM) imaging and Energy Dispersive Spectroscopy (EDS) analysis.

Figures 1, 2, 3, and 4

Chapter 3

Mr. Tuggle preformed the Transmission Electron Microscope (TEM) lift-out and Dr. Winkler assisted with the TEM and EDS analysis.

Chapter 4

Mr. Tuggle contributed to the variable temperature stage design and implementation.

Chapter 5

Dr. Gustafsson, Dr. Lee, and Mr. Can performed the Medium Energy Ion Scattering (MEIS) analyses.

Figure 2

Section 5.4.3

1. Introduction

1.1. Dissertation structure and organization

The structure and organization of the dissertation are as follows:

1. Chapter One describes the significance and motivation of this research.
2. Chapter Two focuses on the evolution of Cs droplets in the Si SIMS crater post Cs^+ bombardment. The results show that Cs droplets form within minutes of atmospheric exposure and hours for pure O_2 exposure under high vacuum ($\sim 10^{-6}$ Torr). In both oxygen environments, the Cs droplets go through multiple morphological changes before arriving in their final structure. The Cs droplets were also exposed to elevated temperatures to study how heat affects the morphology of the droplet. This chapter has been published in *Surface Interface Analysis*.
3. Chapter Three investigates the material dependent behavior of the implanted Cs in Si and InAs. Issues with characterizing the distribution and concentration of the implanted Cs are also addressed. The initial temperature-dependent measurements are conducted to explore the effect heat has on the Cs concentration post bombardment (*ex situ*), as well as *in situ* heating via electron bombardment as a method to alter the Cs concentration during the SIMS analysis. This chapter has been published in *Surface Interface Analysis*.
4. Chapter Four discusses the design and implementation of a custom-built variable temperature stage for our SIMS and a variable temperature sample holder. The stage

produces temperatures ranging from -150 to 300 °C. Novel variable temperature applications are shown. This chapter has been published in the *Journal of Vacuum Science and Technology B*.

5. Chapter Five investigates the temperature-dependent Cs relocation, uptake, and distribution in group III-V and IV materials. Experimental techniques and theoretical modeling are employed to investigate the differences between the two groups. Variable temperature cesium build-up curves are acquired to evaluate temperature as a potential solution to the Cs relocation issue. Additionally, a novel method has been developed to calculate the Cs ionization and neutralization as a function of temperature and Cs fluence. This chapter has been published in the *Journal of Vacuum Science and Technology B*.
6. Chapter Six is the summary and conclusions of the research conducted in this dissertation.

References are listed at the end of each chapter for ease of organization.

1.2. Significance and motivation

Secondary Ion Mass Spectrometry (SIMS) is the only characterization technique that combines parts-per-million to parts-per-billion detection with depth profiling. Due to the excellent chemical sensitivity, SIMS is heavily used in the semiconductor industry for measuring the depth distribution of dopants and impurities. Quantitative SIMS is only possible with standards of the element of interest in the matrix of interest and if the element of interest is present in dilute limit (<1%).[1] If the concentration is greater than

the dilute limit, quantitative SIMS is hampered by the matrix effect, which is a nonlinear relationship between the observed signal and concentration. By combining Cs^+ bombardment with positive secondary molecular ion detection (MCs^+),[2] the matrix effect can be reduced and the linear relationship between signal and concentration can be extended from the dilute limit (<1%) to matrix elements. While the MCs^+ method has been shown to be effective at reducing the matrix effect in some materials,[2] it has been less effective in others.[3] Critical to understanding the materials-based difference in the effectiveness of the MCs^+ technique is a fundamental understanding of the uptake, concentration, and distribution of implanted Cs in the sample under Cs^+ ion bombardment.[4]

The first MCs^+ technique publications dates back to late 1980s,[2,5] and yet the MCs^+ technique is not fully understood. In recent years, there has been renewed interest in the MCs^+ technique with the goal of gaining a greater understanding of the fundamental mechanisms of the technique and how the implanted Cs affects the secondary ion emission processes.[6] Generally, the MCs^+ technique reduces the matrix effect for III-V materials but not for group IV materials. Recent publications have stated that if the Cs coverage is kept below five percent,[6] the matrix effect can be minimized, if not eliminated during the MCs^+ analysis.[7] Nevertheless, the majority of the MCs^+ SIMS research has focused on understanding why the MCs^+ technique fails to remove the matrix-independent ionization in Si and not why the MCs^+ analysis removes the matrix effect for III-V based materials.

In the case of Si, several authors have shown through experimental[6–8] and theoretical[9] work that the implanted Cs is mobile and relocates towards the surface

during Cs^+ bombardment. It is postulated that the increased surface Cs concentration from the relocated Cs causes the MCs^+ technique to fail to remove the matrix effect in Si. However, there is a void in the literature regarding what factors cause Cs to relocate in Si and raises several questions, such as: What causes the implanted Cs to relocate? Is there a method to reduce or eliminate the mobility of Cs? Does Cs relocation occur in other material systems? Generally there is lack of information on how Cs is incorporated and behaves in materials where the MCs^+ analysis successfully reduces the matrix effect.

This research provides new insights for improving the MCs^+ technique and elucidating the Cs mobility. A combination of multiple experimental techniques and theoretical modeling was employed to investigate the differences between the Cs retention, up-take, and distribution in group III-V and IV materials. The use of temperature to control the location and concentration of Cs was discovered during preliminary experiments and warranted an investigation. Therefore, we designed and implemented a variable temperature stage for our SIMS with temperatures ranging from -150 to 300 °C. This enabled us to study the temperature-dependent component of the Cs mobility and the effect it has on the secondary ion emission processes. Additionally, a method was devised to quantify the amount of neutralization and ionization due to the relocated Cs. The results allow for a more thorough understanding of the material dependence on the Cs^+-sample interaction and the temperature component of the Cs mobility.

References

1. C. Magee and M. Frost, *Int. J. Mass Spectrom. Ion Process.* **143,** 29–41 (1995).

2. Y. Gao, *J. Appl. Phys.* **64,** 3760–3762 (1988).

3. H.E. Smith, *J. Vac. Sci. Technol. A Vacuum, Surfaces, Film.* **9,** 1390 (1991).

4. K. Wittmaack, *Surf. Sci.* **606,** L18–L21 (2012).

5. C. Magee, W. Harrington, and E. Botnick, *Int. J. Mass Spectrom. Ion Process.* (1990).

6. K. Wittmaack, *Surf. Sci. Rep.* **68,** 108–230 (2013).

7. K. Wittmaack, *Int. J. Mass Spectrom.* **313,** 68–72 (2012).

8. R. Valizadeh, J.A. van den Berg, R. Badheka, A. Al Bayati, and D.G. Armour, Nucl. Instrum. Meth. B **64**, 609–613 (1992).

9. K. Wittmaack, *Nucl. Instruments Methods Phys. Res. Sect. B Beam Interact. with Mater. Atoms* **267,** 2846–2857 (2009).

2. On the Evolution of Cs Droplets in SIMS Craters

This paper was published in *Surface Interface Analysis* and reprinted with permission.

2.1 Abstract

The evolution of cesium droplets on silicon by Cs ion bombardment has been studied.

For this work, a (100) Si substrate was sputtered with a 5 keV Cs^+ primary ion beam at 45° until steady state was established. The evolution of Cs droplets was investigated under *in situ* O_2 (oxygen jet) and *ex situ* atmospheric exposure conditions for controlled times. Additionally, the effect of sample heating on Cs droplets was also studied. The techniques used to characterize the Cs droplets were scanning electron microscopy with energy dispersive spectroscopy and X-ray photoelectron spectroscopy. Our results indicate that Cs droplets evolve through a series of different morphologies before reaching their final form, and the rate of evolution depends strongly on environment (O_2 or atmosphere) and the length of exposure.

Keywords: SIMS; MCs^+; Cs; Si; Cs oxide; Cs mobility

2.2 Authors and affiliations

Andrew Giordani,[a,b] Jay Tuggle,[a,b] Christopher Winkler,[a] and Jerry Hunter[a*]

[a] Nanoscale Characterization and Fabrication Laboratory, Virginia Tech, 1991 Kraft Drive, Blacksburg, VA, USA

[b] Department of Materials Science and Engineering, Virginia Tech, 445 Old Turner Street, Blacksburg, VA, USA

* Corresponding author e-mail: hunterje@vt.edu

2.3 Introduction

The use of Cs bombardment in secondary ion mass spectrometry (SIMS) has long been known to enhance negative ion yields[1] and reduce the SIMS matrix effect enabling

composition measurements (>1 at.%).[2] However, there are several issues associated with Cs bombardment, including the mobility of Cs and the influence oxygen has on altering the location and concentration of the Cs during bombardment.[3] Exposing the Cs sputter crater to atmosphere post bombardment also affects the location and concentration of Cs, which makes characterization of the implanted Cs difficult.[4-6] An additional effect of exposing the Cs sputter crater to atmosphere is the formation of Cs droplets in and around the sputter crater.[5-7] It was previously established by Gries[8] that Cs droplets readily form at dislocation sites from Cs ion bombardment. Therefore, when a Cs^+ ion encounters a dislocation site it loses its polarity and becomes trapped, creating a nucleation site where Cs^+ ions can agglomerate and form Cs droplets.[8] Further studies have shown that Cs droplets have several different oxidation states and form on a variety of samples, both organic[7] and inorganic.[6]

Still there is a gap in the literature on understanding how the Cs droplet evolves into their final structure, even though the formation of Cs droplets has been known for some time.[6] Therefore, the focus of this paper is to study how Cs droplets evolve on Si exposed to atmosphere and pure oxygen post bombardment. An additional aspect of this paper is to investigate the effect heat has on Cs droplets. From these results, we gain a greater knowledge of Cs droplets and can take the appropriate actions to avoid the formation of Cs droplets.

2.4 Experimental

A clean (100) Si substrate was bombarded with a 5 keV Cs^+ ion beam at 45° in Cameca IMS-7f Geo (positive mode). A well-focused 50 nA ion beam was rastered over

a 250 × 250 μm area to produce a flat-bottom crater. All craters in this study were sputtered under an oxygen leak (main chamber pressure of $3x10^{-6}$ Torr) to increase the near surface Cs concentration.[3] Steady state was achieved to ensure that all craters had the same Cs concentration, as indicated by the Cs^+ secondary ion signal.

After bombardment, the freshly sputtered craters were either exposed to *in situ* O_2 (oxygen leak), atmosphere, or atmosphere followed by vacuum heat treatment for controlled times. Heating was performed on the hot stage in a Phi Quantera SXM X-ray Photoelectron Spectrometer (XPS) under vacuum ($<2x10^{-8}$ Torr). The location and morphology of Cs droplets were characterized either on an FEI Quanta 600 FEG Scanning Electron Microscopy (SEM) or an FEI Helios 600 NanoLab Dual Beam, and elemental information was obtained from a Bruker QUANTAX 400 Energy Dispersive Spectrometer (EDS) and XPS.

2.5 Results and discussion

2.5.1 Atmospheric evolution of Cs droplets

A freshly sputtered Si crater was exposed to atmosphere for controlled times to monitor the evolution of Cs droplets in the crater bottom. After sputtering, the sample was immediately transferred to the SEM and atmosphere was introduced by venting the chamber for controlled times. One Cs droplet was monitored in the SEM as the atmospheric exposure increased by marking the stage position. Figure 1 shows the evolution of the Cs droplet in atmosphere. Cs droplets began to form after 4 min of atmospheric exposure with a relatively large droplet diameter, ~2 μm (Fig. 1a). After 4 min of atmospheric exposure, the droplet was of sufficient size to determine the

composition using EDS.[9] The EDS spectrum, generated using a 15 keV electron beam (Fig. 2), had clearly defined Cs peaks, which confirmed the presence of Cs in the droplet. As the atmospheric exposure increased, the large diameter droplet condensed into one small droplet (Fig. 1b and 1c), collapsed (Fig. 1d), and then reformed (Fig. 1e). The final monitored form occurred at 18h of atmospheric exposure and appeared to have a distinct shape with faceted sides (Fig. 1f). A possible explanation for the different structural forms of the Cs droplet could be various forms of Cs oxide; however, further experiments would need to be conducted to confirm that hypothesis.

As a result of this SEM atmospheric exposure study, it is concluded that any *ex situ* characterization of Cs is questionable due to the fact that Cs readily forms droplets within minutes of atmospheric exposure. Therefore, if characterization of Cs is desired, it is essential to minimize atmospheric exposure or to transfer under an inert atmosphere or vacuum.

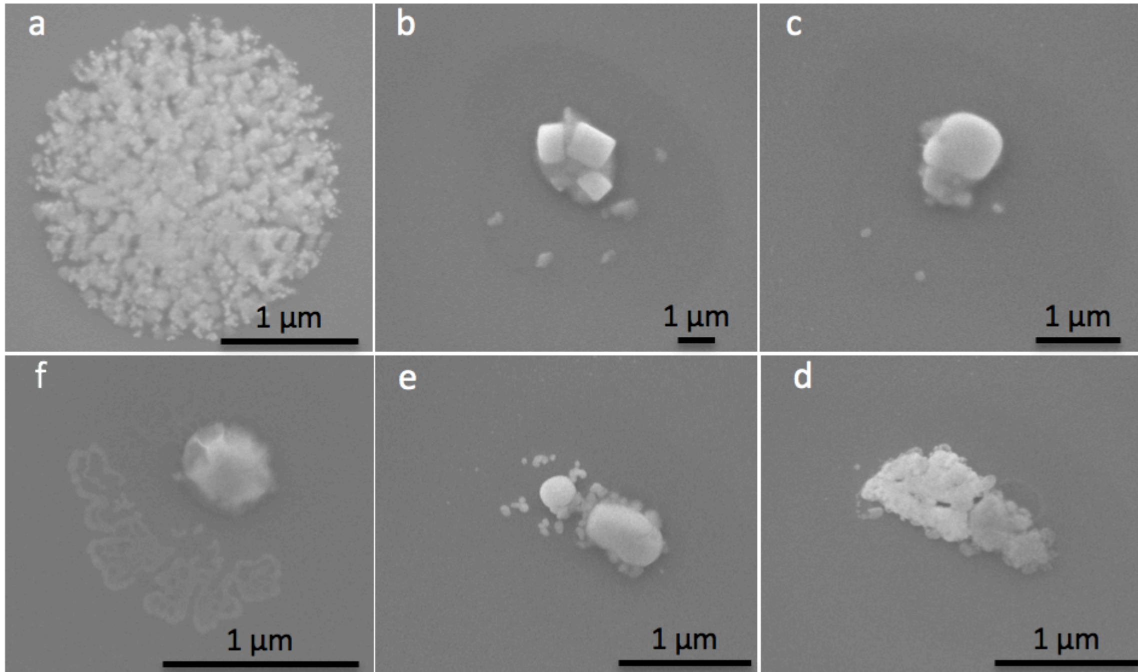

Figure 1. Evolution of Cs droplets as a function of atmospheric exposure; a: 4 min; b: 8 min; c: 18 min; d: 25 min; e: 60 min; f: 18 h.

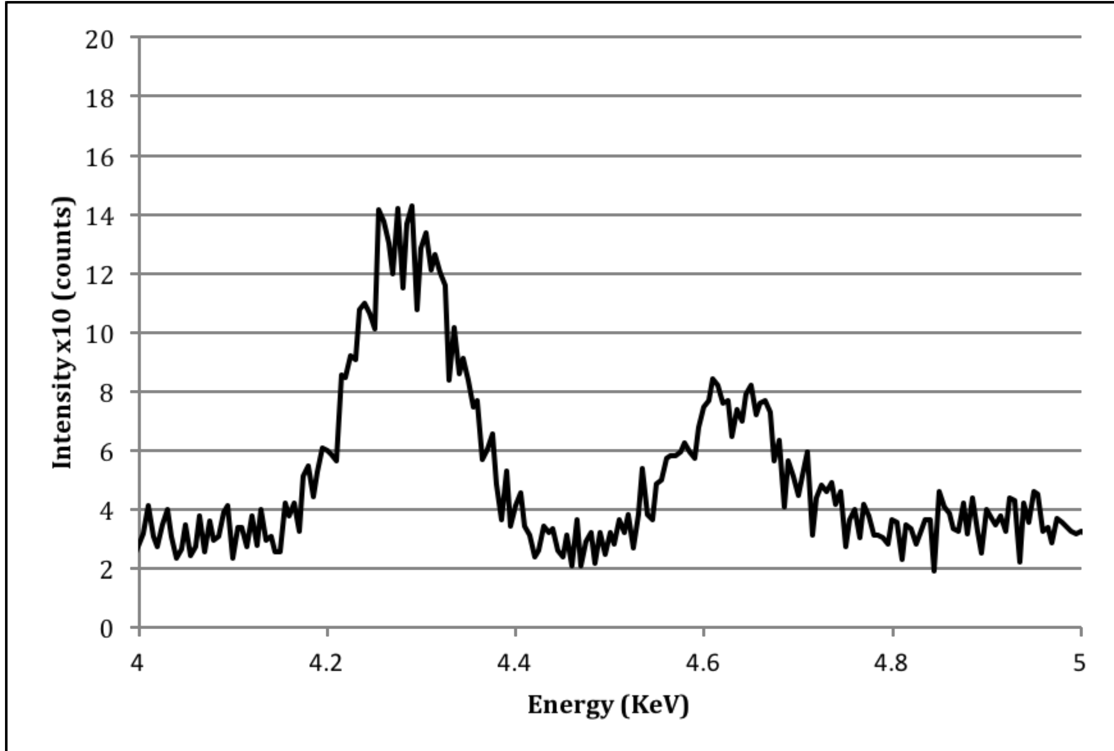

Figure 2: EDS spectrum of the CsLα (4.29 keV) and CsLβ (4.62 keV) from the Cs droplet in Fig. 1a, confirming the presence of Cs in the droplet.

2.5.2 O_2 evolution of Cs droplets

The O_2 exposure experiment was conducted by sputtering multiple craters and further exposing the sputter craters to an oxygen leak for controlled times. An immediate transfer to SEM then allowed for a study of the evolution of the Cs droplets. The purpose of O_2 exposure was expected to reduce the pace at which Cs droplets form in order to better observe the structural changes. The first Cs droplets appeared after 2 h of O_2 exposure. The length of time for initial droplet formation is attributed to the low partial pressure of O_2, $3x10^{-6}$ Torr, in the SIMS chamber. Fig. 3 illustrates the evolution of Cs droplets in a pure oxygen environment. Please note that Fig. 3 is not the same Cs droplet, but the average shape of the Cs droplets in the sputter crater. The initial Cs droplets appeared triangular in shape (Fig. 3a), but as the O_2 exposure increased, the Cs droplets separated (Fig. 3b) and then flatten into various elongated structures (Fig. 3c). After 4 h of O_2 exposure, the Cs droplets were in their final form (Fig. 3d) and uniformly spread across the crater bottom with a diameter of ~150 nm. Both the O_2 and atmospheric formed Cs droplets went through similar structural changes; however, the rate of structural change in the O_2 formed Cs droplets was much slower.

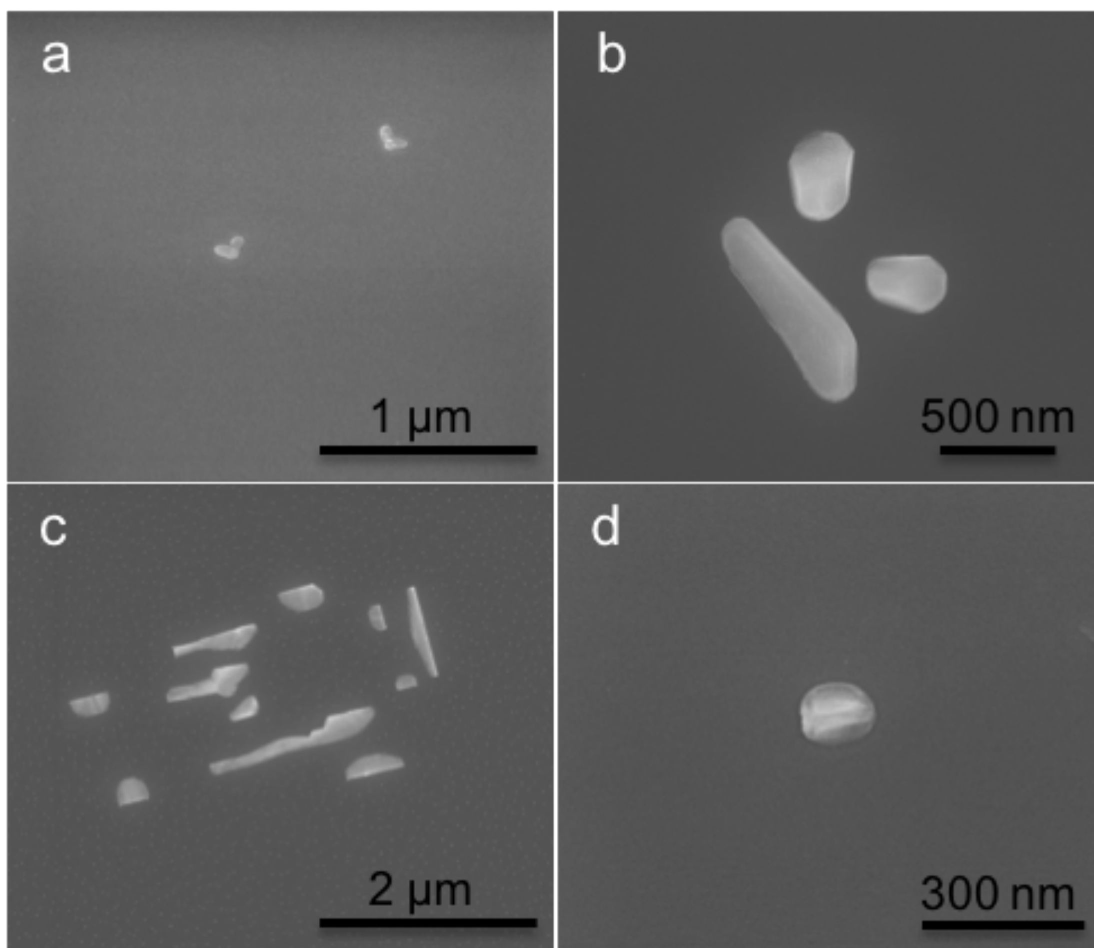

Figure 3. Evolution of Cs droplets with increasing O_2 exposure; a: 2 h; b: 2.5 h; c: 3 h; d: 4 h.

2.5.3 The effect of heat on Cs droplets

No Cs droplets were present when imaging a newly formed Si sputter crater with <1 min atmospheric exposure in the SEM. After the Si sputtered crater was exposed to atmosphere for 10 min and reimaged, Cs droplets appeared everywhere except in the area that had been previously rastered with the electron beam. From this observation, it was hypothesized that heat generated from the electron beam increased the mobility of Cs and rastering of the electron beam 'swept' the Cs from the rastered area. To test this

hypothesis, the effect heat had on the already formed Cs droplets was investigated. The heat experiment was carried under vacuum (<$2x10^{-8}$ Torr) in the XPS using a heated specimen stage. Prior to heating, the sputter crater was exposed to atmosphere for 4 h to allow Cs droplets to form (Fig. 4a). The Si crater was heated to 250 °C and held for 1 h then immediately transferred into the SEM to be imaged. Figure 4b shows the influence that heat has on the Cs droplets. The heated Cs droplet (Fig. 4b) lost all structure and appeared to be flat in comparison with the non-heated Cs droplet. Please note that these are different droplets, but represent the average structure of the Cs droplets in the crater. In addition, XPS was used to analyze before and after heating, and the results show a lower atomic concentration of Cs after heating at 250 °C for 1 h. The XPS results for before heating are Cs: 7.1 at.% Si: 36.7 at.% O: 56.2 at.% and Cs: 6.1 at.% Si: 39.0 at.% O: 54.9 at.% for 1 h of heating at 250 °C. At this point, it is uncertain whether the difference in the XPS measured Cs concentration is a real change in Cs concentration or an artifact in the XPS measurement due to a change in morphology (Fig. 4).

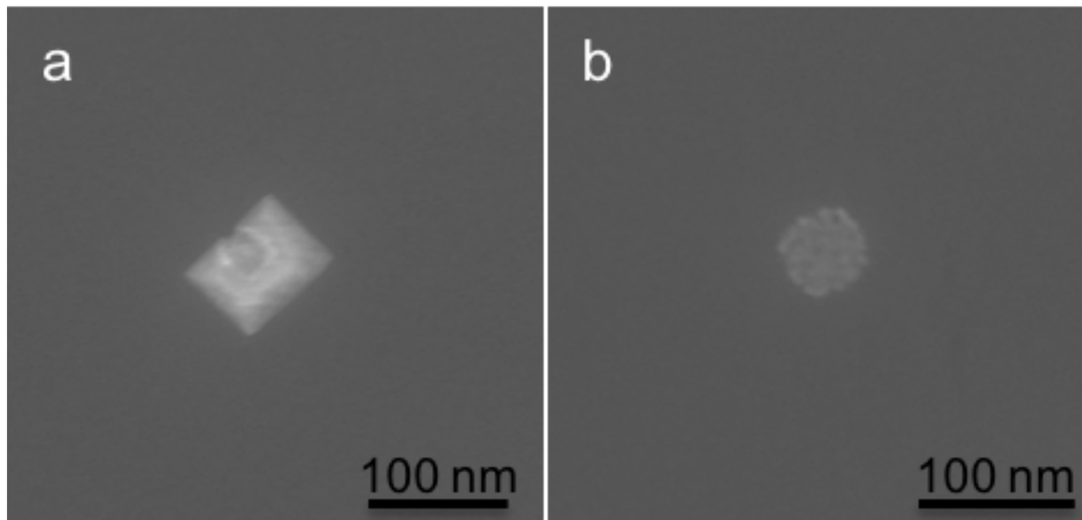

Figure 4: Effect of sample heating on Cs droplets; a: 4 h of atmospheric exposure – no heat; b: 4 h of atmospheric exposure followed by 250 °C for 1 h.

2.6 Conclusion

This study confirms that Cs is mobile within the SIMS crater and that Cs droplets form when exposed to oxygen (O_2 or atmosphere). Also, Cs droplets evolve as a function of oxygen (O_2 or atmosphere) exposure and go through a series of different morphologies before arriving in their final form. It was also concluded that Cs droplets are affected by heat, either from the electron beam in the SEM or by conduction heating on a vacuum hot stage. The readily formed Cs droplets in atmosphere and the mobility of Cs may have an effect on the ability to characterize the implanted Cs; therefore, to properly characterize the implanted Cs one should avoid any oxygen exposure.

2.7 Acknowledgements

The authors would like to thank the Institute for Critical Technology and Applied Science and the Nanoscale Characterization and Fabrication Labs at Virginia Tech for

support and funding.

References

[1] V.E. Krohn, J. Appl. Phys. **1962**, 33, 3523.

[2] Y. Gao, J. Appl. Phys. **1988**, 64, 3760.

[3] N. Menzel, Nucl. Instruments Methods Phys. Res. **1981**, 191, 235.

[4] A. Mikami, T. Okazawa, Y. Kido, Jpn. J. Appl. Phys. **2008**, 47, 2234.

[5] K. Wittmaack, Surf. Sci. Rep. **2013**, 68, 108.

[6] W.H. Gries, J. Vac. Sci. Technol. A Vacuum, Surfaces, Film. **1987**, 5, 1740.

[7] K. Ngo, P. Philipp, J. Kieffer, T. Wirtz, Surf. Sci. **2012**, 606, 1244.

[8] K. Miethe, W.H. Gries, A. Pocker, **1992**, SIMSVIII, 347.

[9] J. Goldstein, D. Newburry, D. Joy, C. Lyman, P. Echlin, E. Lifshin, L. Sawyer, J. Michael, *Scanning Electron Microscopy and X-ray Microanalysis*, Plenum, New York, **2003**, 217–295.

3. Temperature Dependent Relocation of the Cesium Primary Ion Beam During SIMS Analysis

This paper was published in *Surface Interface Analysis* and reprinted with permission.

3.1 Authors and affiliations

Andrew Giordani,[a,b] Jay Tuggle,[a,b] Christopher Winkler,[a] and Jerry Hunter[a*]

[a] Nanoscale Characterization and Fabrication Laboratory, Virginia Tech, 1991 Kraft Drive, Blacksburg, VA, USA

[b] Department of Materials Science and Engineering, Virginia Tech, 445 Old Turner Street, Blacksburg, VA, USA

* Corresponding author e-mail: hunterje@vt.edu

3.2 Abstract

The ability to control and accurately measure the cesium concentration, [Cs], is a critical step toward understanding the role of Cs in the SIMS MCs^+ technique. We have developed a method to alter the instantaneous [Cs] by using electron gun heating (*in situ*) during Cs bombardment and found that heating (*ex situ*) during the X-ray Photoelectron Spectroscopy (XPS) analysis provides a qualitative depth distribution of the implanted Cs. The effectiveness of *in situ* and *ex situ* heating is explored on (100) silicon and (100) indium arsenide. Cs build-up curves are studied to determine if *in situ* heating produces secondary ion yields that are favorable for the MCs^+ technique. In addition to XPS, Scanning Electron Microscopy/Energy Dispersive Spectroscopy (SEM/EDS) and Scanning Transmission Electron Microscopy/Energy Dispersive Spectroscopy (STEM/EDS) are utilized to measure [Cs]. The goal of this work is to improve the quantification of the MCs^+ technique used in SIMS by understanding the material

dependent behavior (incorporation and retention) of Cs and how it affects the MCs^+ analysis.

Keywords: SIMS, MCs^+, Cs, Electron Heating, Cs Mobility, Cs retention

3.3 Introduction

SIMS is the only characterization technique that combines parts-per-million to parts-per-billion detection with depth profiling. Because of the excellent chemical sensitivity, SIMS is heavily used in the semiconductor industry for measuring the depth distribution of dopants and impurities. SIMS has long been hampered by the 'matrix effect' that leads to improper quantification of impurities outside the dilute limit (<1 at.%). The MCs^+ method has proven to be successful at minimizing matrix effects in III–V compound semiconductors,[1,2] but less effective in Si and other group IV compounds.[3,4] Critical to understanding this material dependence is knowledge of the concentration of retained Cs in the sample,[5] *i.e.* the instantaneous surface Cs concentration, [Cs], and how that affects the MCs^+ formation.

A major issue with the MCs^+ technique is that, under typical analysis conditions, Cs overloading of the sample surface can occur nearly immediately, and once the analysis area is saturated or overloaded with Cs, the excess Cs limits the ionization efficiency of Cs^+ causing a reduction in the Cs^+ ion yield. This phenomenon is known to occur in Si[6] and may be the reason the MCs^+ technique does not reduce the matrix effect in Si. Recent work suggests if the Cs coverage, during the SIMS analysis, is kept below 5%, the 'matrix effect' can be minimized if not eliminated for the MCs^+ technique.[5,6] Therefore, several techniques have been investigated and/or developed to minimize the

instantaneous [Cs]. Co-sputtering[7] and neutral Cs deposition[8] have been developed to control the instantaneous [Cs], but these instrument modifications are not routinely available for the Cameca IMS SIMS instruments (CAMECA Instruments, Inc., Madison, WI). Varying the angle and energy of the primary ion beam has also been used to control the instantaneous [Cs].[3] However, on Cameca IMS type SIMS instruments, angle and energy are coupled, limiting the achievable energy/angle range and therefore the [Cs]. Oxygen flood (O_2 jet) has also been investigated as means to control the instantaneous [Cs], but Vandervorst[9] concluded that using the O_2 jet during the analysis increases the [Cs] which is opposite to the desired reduction of the [Cs] for improving the MCs^+ analysis.

One potential route to alter the instantaneous [Cs] meriting study is to heat the sample during analysis. The sample was heated by bombarding the analysis area with electrons[10] from the Normal-incidence Electron Gun (NEG), which are readily available on many Cameca IMS type instruments. The heat generated from the NEG was relatively low with compared with rapid thermal annealing temperatures and therefore should not distort the distribution of implanted elements in the sample. The focus of this paper is on altering the instantaneous [Cs] by applying heat during Cs bombardment and studying the effect of heat on the implanted Cs post-bombardment. Also, the effect of heat on Cs^+ secondary ion yields will be discussed.

3.4 Experimental

Semiconductor grade (100) Si and (100) InAs substrates were chosen for this study. Cs ion implantation was performed using a Cameca IMS-7f Geo. A well focused 50 nA,

5 keV Cs^+ ion beam at 45°, was rastered over a 300 x 300 μm area to form a flat bottom crater. A 1 nA beam was used when studying how the secondary ion yields vary as a function of Cs fluence (cesium build-up curves). All SIMS craters were sputtered until steady state was achieved as indicated by monitoring the Cs^+ ions.

In situ heating was accomplished by bombarding the surface with 7 keV electrons from the NEG. The NEG current controls the sample temperature, *i.e.* increasing the current increases the sample temperature. Because of the lack of a thermocouple on the sample stage, it was not possible to make a direct measurement of the sample temperature during analysis, so the actual temperature in the analysis area was unknown. An ~300 μm diameter NEG beam was aligned and focused[11] directly over the analysis area to encompass the crater, and the following electron current densities were used: 0 (no heat or regular), 15, 140, 280, and 640 $\mu A/cm^2$ as measured by absorbed electron current on the sample holder.

Ex situ heating was performed on the hot stage in a Phi Quantera SXM X-ray Photoelectron Spectrometer (XPS). XPS measurements were performed at 23, 50, 100, 150, 200, and 250 °C (maximum achievable temperature). Once the set temperature was achieved, the sample was allowed to equilibrate for 5 min prior to the start of the XPS analysis. The XPS atomic concentrations were calculated by multiplying the background subtracted photoelectron peak areas by their relative sensitivity factor. Several electron spectroscopy techniques were additionally employed to provide elemental information on the sputter crater, such as Scanning Electron Microscopy/Energy Dispersive Spectroscopy (SEM/EDS; FEI Quanta 600 SEM equipped with a Bruker QUANTAX 400 EDS FEI Quanta 600, FEI, Hillsboro, OR) and Scanning Transmission Electron

Microscopes/Energy Dispersive Spectroscopy (STEM/EDS; JEOL 2100, JEOL USA, Inc., Peabody, MA).

3.5 Results and discussion

3.5.1 Behavior of Cs

We investigated the material dependent behavior of the implanted Cs in Si and InAs. Previous work has shown that Cs bombarded Si samples are strongly affected by the presence of oxygen and form Cs rich droplets when exposed to atmosphere.[12,13] To determine if Cs in InAs behaves in a similar manner to Cs in Si, we exposed Cs-sputtered InAs craters to atmosphere and vacuum (<5x10^{-8} Torr) for controlled times and measured the [Cs] with XPS. In the case of Si, when stored in vacuum for 24 h, the [Cs] remained constant (4.8 at.%) compared with 24 h of atmospheric exposure, the [Cs] decreased by 8% to 4.4 at.%. The Cs–Si interaction with oxygen is discussed elsewhere in greater detail.[13] However, this trend did not occur in InAs, and the measured [Cs] increased under both, vacuum and atmospheric, exposure conditions with time from 2.1 to 2.9 at.% and 2.0 to 2.6 at.%, respectively. The increase of [Cs] in InAs may be attributed to the migration of Cs to the surface.

The change in measured [Cs] may not be a true increase or decrease but an artifact of the XPS measurement caused by a change in the surface distribution of Cs (formation of Cs droplets). We expect the [Cs] to decrease with the formation of sufficiently large Cs droplets because the information depth of XPS, under these conditions, is fixed and the implanted Cs has relocated above the surface as Cs droplets; effectively lowering the measured [Cs], even though the total amount of implanted Cs is unchanged. It is worth

noting that the XPS information depth for Cs in Si is ~10 nm and ~7 nm for InAs. Also, there is a factor of 3 difference in sputter yield between Si and InAs under these conditions, 4.0 and 12.4, respectively. This explains the difference in the measured [Cs] between InAs and Si, as predicted by the sputter yield approximation.[6] These results show a material dependence on the incorporated and retained Cs under different exposure conditions with time. If any post-bombardment characterization is desired, the sample should be transferred under vacuum[14] or in an inert atmosphere and performed immediately to avoid further complications.

3.5.2 Measuring Cs concentration

XPS, SEM/EDS, and STEM/EDS were used to characterize the surface, lateral, and in-depth distribution of Cs in the crater bottom. The variety of characterization techniques employed reflects both the difficulty of measuring the three-dimensional concentration of Cs and the limitations of each individual technique. SEM/EDS results were erroneous, because of the large difference in analysis volume compared with the Cs implant depth. Any attempt to characterize the Cs droplets formed on the Si crater bottom[12] with SEM/EDS was also complicated by the electron beam causing the droplet to dissolve back into the Si matrix. This droplet dissolution induced by the electron beam made any analysis technique suspect that used an electron beam as the probing source. STEM/EDS was used to measure the [Cs] as a function of depth by analyzing a cross-section of the SIMS sputter crater prepared on a Dual Beam FEI Helios 600 NanoLab. The STEM/EDS map clearly showed the interface between the sputter beam and matrix; however, Cs was not detected, even for long count times. XPS and SEM/EDS data confirm the presence of Cs in the sample as a result of Cs bombardment. Therefore, the

lack of Cs in the STEM/EDS map was either an artifact of sample preparation or an electron beam-induced effect, similar to those observed in the SEM. If the retained Cs was mobile under the electron beam, the additional two free surfaces of the TEM sample are expected to more easily allow Cs to escape. To solve the Cs detection issue in TEM, other methods for sample preparation will be explored, such as the small angle cleavage technique.[15] Thus far, XPS has been the most successful characterization technique by providing the concentration of the implanted Cs in the crater bottom. The biggest difficulty with XPS is the brief, but unavoidable atmospheric exposure during transfer between instruments in our laboratory.

3.5.3 The effect of heat of Cs concentration

The effect of *in situ* heating on altering the instantaneous [Cs] in Si and InAs was investigated. The first experiment was to determine the effect that changing the current density of the NEG (increasing the temperature) while simultaneously sputtering had on the surface [Cs]. The initial results indicate that NEG-heating increases the surface [Cs]. At an electron current density of 15 $\mu A/cm^2$, the measured [Cs] increased from 2 to 6 at.% in InAs and increased slightly in Si from 4.7 to 5.0 at.%. At NEG current densities >15 $\mu A/cm^2$, the [Cs] returned to the same [Cs] as the regular (no NEG) sputtering condition and remained unchanged as the electron current density was increased up to 640 $\mu A/cm^2$.

We hypothesize that the increase in instantaneous [Cs] during electron bombardment heating is purely a thermal mechanism. Heat generated from the NEG enhances the mobility of the implanted Cs causing the implanted Cs to migrate toward the surface

during Cs bombardment. This assertion is confirmed by comparing the sputter yields of InAs under regular (no NEG) and NEG heat (140μA/ cm^2 electron current density) during sputtering, which are 12.4 and 7.0, respectively. The difference in sputter yields indicates an increase in sputtering of the mobile implanted Cs relative to the InAs matrix. The sputter yield for Si showed a slight decrease from 4.0 to 3.9 with NEG-heating, which is in agreement with the other heating experimental results for Si.

To understand the effect heat has on the implanted Cs and to decouple the effect electron bombardment may have on the [Cs], we heated the sample post-bombardment (*ex situ*) in the XPS and measured the [Cs] as function of temperature (Fig. 1). InAs showed a significant increase in measured [Cs] between 50 and 100 °C compared with Si, where the [Cs] gradually increased with temperature. The *ex situ* heating results not only show that the implanted Cs is mobile at elevated temperatures but also provides a qualitative depth distribution of the retained Cs. We also conducted an experiment to determine if NEG heating alters the [Cs] in the sample by *ex situ* heating samples that had been previously NEG-heated during SIMS bombardment. Figure 1 shows that the NEG-heated [Cs] for InAs was unaffected as temperature increased compared with the non NEG-heated InAs [Cs]. This indicates that the majority of the implanted Cs from the NEG-heating is located at or near the surface as compared with regular (no NEG) sputtering where the majority of the implanted Cs remains in the sample. To further illustrate the effect that NEG-heating had on the [Cs], the following set of experiments were conducted, and the resulting [Cs] were measured: (1) simultaneous (Cs bombardment with NEG) heating results in 2 at.% [Cs], (2) Cs bombardment followed by NEG-heating results in 5 at.% [Cs], and (3) simultaneous heating followed by NEG-

heating results in 2 at.% [Cs]. These results show that lowering the XPS measured [Cs] requires ion bombardment in combination with NEG-heating and that NEG-heating alone increases the instantaneous surface [Cs] during the SIMS analysis as previously shown in the *ex situ* XPS-heated experiment.

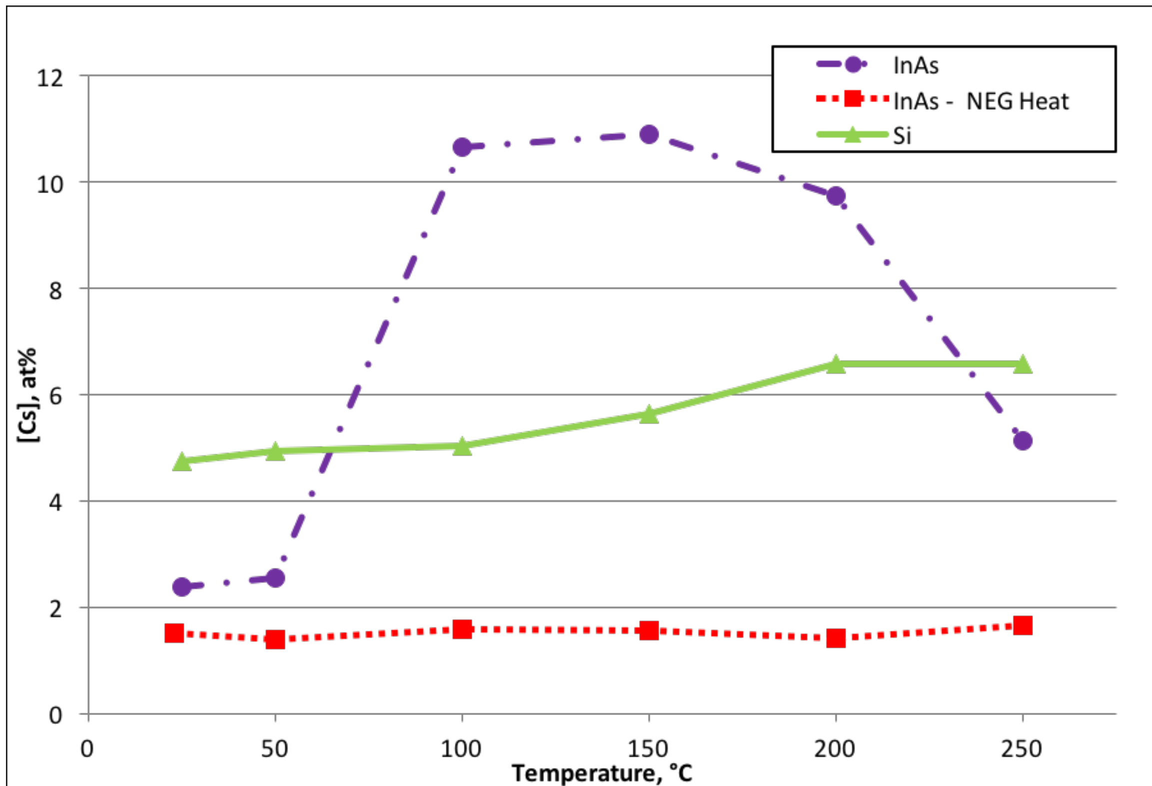

Figure 1: XPS measured [Cs] as a function of temperature on InAs and Si. Illustrating the effect sample heating has on the implanted Cs and difference in retained Cs between InAs and Si. The effect that NEG (*in situ*) heating has on the distribution of the implanted Cs in InAs is also shown.

3.5.4 Effect of heat on Cs^+ ion yield

The MCs^+ technique requires low surface [Cs] and a constant emission of Cs^+ secondary ions; otherwise, the MCs^+ technique will not reduce the matrix effect.[6] Cs build-up curves were acquired for Si and InAs under regular and NEG-heated sputtering conditions to determine how Cs was incorporated into the sample and its effect on the

secondary ion yields. The Cs build-up curve for InAs shows a constant emission of Cs^+ secondary ions as the Cs fluence increases (Fig. 2), illustrating no Cs overload. This type of Cs^+ secondary ion yield is conducive for the MCs^+ technique, which can be attributed to high sputter yield of InAs, and also explains why matrix composition measurements are possible with the MCs^+ technique. However, the Cs build-up curve for in situ NEG-heated InAs shows an overload of Cs^+ and a reduction in the Cs^+ secondary ion yield. The difference in the Cs build-up curves can be explained by the increased instantaneous surface [Cs] from *in situ* heating. *In situ* heating causes the implanted Cs to become mobile and move to the sample surface resulting in an overload of Cs and limiting the emission of Cs^+ secondary ions. The Cs build-up curves for Si are not shown here, but both the *in situ* heated and non-heated result in a significant overload of the surface with Cs and the resultant reduction in the Cs^+ ion emission as discussed earlier. The low sputter yield of Si, 4, may explain why there was an excess amount of Cs at the surface (Cs overload) and why the MCs^+ does not reduce the matrix effect for Si. By measuring Cs build-up curves, we confirmed that *in situ* heat increases the instantaneous [Cs] and conclude that *in situ* heating was not advantageous for the MCs^+ technique.

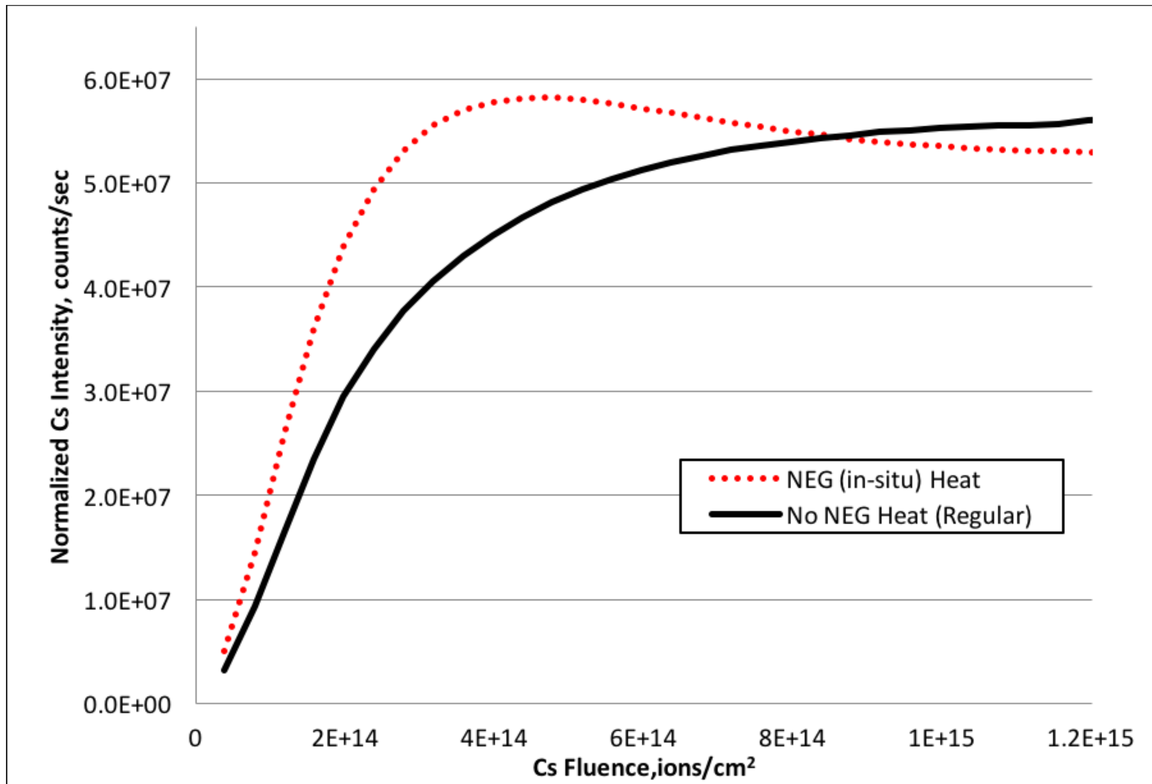

Figure 2: SIMS build up curve for InAs under regular and 640 µA/cm^2 NEG heated Cs^+ primary ion bombardment.

3.6 Conclusion

We demonstrated a method for altering the [Cs] on a Cameca IMS-7f Geo by NEG-heating while simultaneously sputtering with Cs with the intent of improving the quantification of MCs^+ technique. However, *in situ* heating with the NEG has proven to be an unsuccessful method for lowering the instantaneous [Cs] and, as a result, did not produce Cs^+ secondary ion yields that were conducive for the MCs^+ technique. Several issues with characterizing the implanted Cs have been discussed, especially with electron-based techniques, and XPS has proven to be a more reliable method for quantifying the surface [Cs] versus the other techniques studied. *Ex situ* heating

confirmed that more Cs was retained in InAs than Si. The results from this study clearly indicate a material-based difference in the amount of incorporated Cs and could be the defining issue of why the MCs^+ technique reduces the matrix for some materials and not for others.

3.7 Acknowledgements

The authors would like to thank the Institute for Critical Technology and Applied Science and the Nanoscale Characterization and Fabrication Labs at Virginia Tech for support and funding.

References

[1] Y. Gao, *J. Appl. Phys.* **1988**, 64, 3760.

[2] C.W. Magee, W.L. Harrington, E.M. Botnick, *Int. J. Mass. Spectrom. Ion Processes* **1990**, 103, 45.

[3] K. Wittmaack, *NIM B* 1994, 85, 374.

[4] H. E. Smith, B. H. Tsao, J. Scofield, *Silicon Carbide and Related Materials* 2005 2006, 527, 629.

[5] K. Wittmaack, *Surf. Sci.* **2012**, 606, L18.

[6] K. Wittmaack, Surf. Sci. Rep. **2013**, 68, 108.

[7] J. Brison, L. Houssiau, *NIM B* **2007**, 259, 984.

[8] T. Wirtz, H.-N. Migeon, *Appl. Surf. Sci.* **2004**, 231, 940.

[9] B. Berghmans, J. Rip, W. Vandervorst, *Surf. Interface Anal.* **2001**, 43, 225.

[10] R. Castaing, *Ph.D. Thesis*, University of Paris **1951**.

[11] A. L. Pivovarov, F. A. Stevie, D. P. Griffs, *Appl. Surf. Sci.* **2004**, 231, 786.

[12] A. Giordani, J. Tuggle, C. Winkler, J. Hunter, Submitted to *Surf. Interface Anal.* November **2013**.

[13] K. Q. Ngo, P. Philipp, J. Kieffer, T. Wirtz, *Surf. Sci.* **2012**, 606, 1244.

[14] B. Bendler, R. Barrahma, P. Philipp, T. Wirtz, *Surf. Interface Anal.* **2011**, 43, 514.

[15] S. D. Walck, J. P. McCaffery, *Thin Solid Films* **1997**, 308, 399.

4. Design and Implementation of a Custom Built Variable Temperature Stage for a Secondary Ion Mass Spectrometer

This paper was published in the *Journal of Vacuum Science and Technology B* and reprinted with permission.

4.1 Authors and affiliations

A. Giordani[1,2], J. Tuggle[1,2], J. Hunter[1,3,a)]

[1] Nanoscale Characterization and Fabrication Laboratory, Virginia Polytechnic Institute and State University, 1991 Kraft Dr., Blacksburg, Virginia 24060

[2] Department of Materials Science and Engineering, Virginia Polytechnic Institute and State University, 445 Old Turner St., Blacksburg, Virginia 24060

[3] Materials Science Center, University of Wisconsin-Madison, 1509 University Avenue, Madison, Wisconsin 53706

[a)] Electronic mail: jerry.hunter@wisc.edu

4.2 Abstract

The authors have built, designed, and implemented a variable temperature stage for a Cameca IMS 7f-GEO with an achievable temperature range of -150 to 300 °C and designed a new sample holder for rapid thermal stabilization. This paper focuses on the design and implementation aspects of the variable temperature stage in detail. The authors demonstrate applications where temperature control is useful for analyses that are not possible at room temperature.

4.3 Introduction

Secondary ion mass spectrometry (SIMS) is a technique widely used across many science and engineering disciplines for obtaining trace elemental or molecular information (ppm- ppb). SIMS is also a versatile technique with several analysis modes such as mass spectra, depth profiling, and ion imaging. The limitation of SIMS is that most measurements are made at room temperature, and, in some cases, it would be beneficial to operate it at either elevated or cryogenic temperatures. Therefore, adding a variable temperature stage to the instrument would increase the usefulness of the technique and enable measurements that are not possible at room temperature. For

example, cooling the sample to cryogenic temperatures permits the analysis of biological samples[1] and fluid melt inclusions;[2] heating the sample allows high temperature phase transformations to be analyzed;[3] and, utilizing both cryogenic and elevated temperatures enables temperature dependent[4,5] and diffusion studies. Additionally, a variable temperature stage may be useful for improving the vacuum conditions by either quickly outgassing a sample at elevated temperatures or reducing the outgassing rate at cryogenic temperatures. Our primary need for a variable temperature stage is to study the temperature-dependent relocation of the Cs^+ primary ion beam during the SIMS analysis.[4,5] This paper focuses on the design and implementation of a variable temperature stage and sample holder for a Cameca IMS 7f-GEO. We demonstrate several novel applications that utilize the variable temperature stage. This is not the first variable temperature stage for a Cameca SIMS,[1-3] but the complexity of the Cameca IMS 7f-GEO main chamber and motorized stage requires a novel approach.

4.4 Design requirements

The variable temperature stage had several design requirements: (1) preserve the original operation and functionality of the instrument [*i.e.*, focusing of the secondary ion optics, loading and unloading the sample, and maintaining a constant distance (4.5 mm) between the immersion lens and sample during operation]; (2) compatible with the existing stage assembly for minimal instrument alterations; (3) ensure that all components are ultrahigh-vacuum compatible to maintain the existing vacuum (8×10^{-10} Torr); (4) able to float at the sample bias (±5 kV with respect to ground); and (5) achieve and maintain sample temperatures from near-liquid nitrogen temperatures to 300 °C

during operation.

4.5 Design and implementation

Figure 1 shows the variable temperature stage assembled on the main chamber door. The following design and implementation discussion is divided into three sections: (1) stage components; (2) stage electronics; and (3) sample holder.

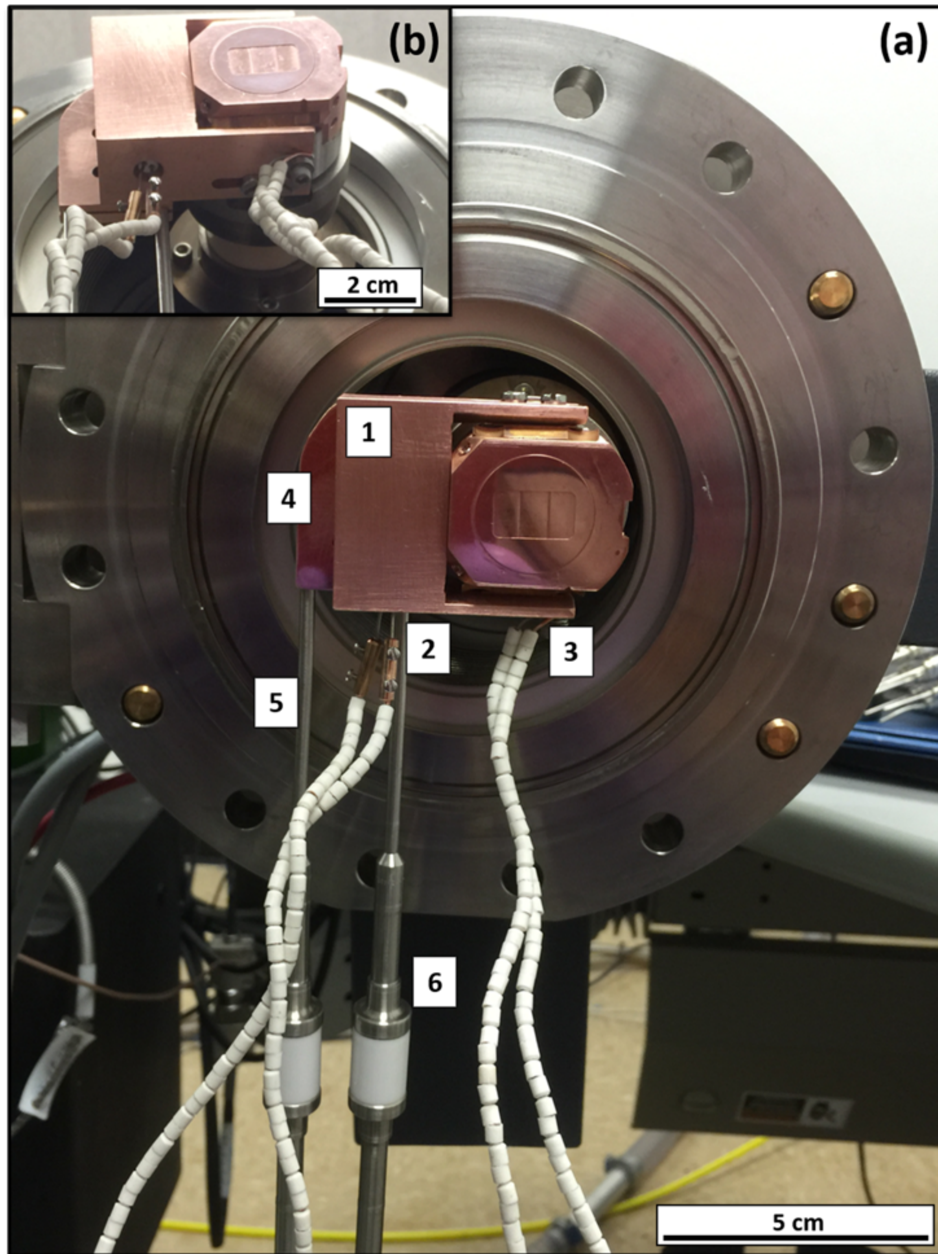

FIG. 1. (Color online) (a) Variable temperature stage assembled with main chamber door open. (b) Bottom view to show connections.

4.5.1 Stage components

The variable temperature stage has two main structural components: (1) the heater block (number 1 in Fig. 1) that contacts the sample holder to deliver the desired

temperature through conduction; and (2) the cryogenic block (number 4 in Fig. 1) which is attached to the back of the heater block. The heating and cryogenic blocks work in tandem to provide a wide range of temperatures and are made of oxygen-free, highly conductive copper to ensure high thermal conductivity and limited vacuum contamination. The heater block is designed to easily attach to the existing stage assembly with the screws that attach the sample holder clips to the stage assembly [see Fig. 1(a)]. By attaching the variable temperature stage to the existing stage assembly, the full X-Y-Z movement of the stage is preserved as if the variable temperature stage was not attached. This is very important because the X and Y movement of the stage is motorized, and the Z position of the stage could vary slightly due to the thermal contraction or expansion of the stage assembly during heating or cooling. To further ensure that the stage has full X-Y range of motion, the cryogenic trap assembly was removed. The stainless steel bellows connected to the cryogenic block function as a cryogenic trap, alleviating the need for the existing cryogenic trap.

All of the cryogenic and electrical connections were made using a four-way reducing cross because of the limited space and useable ports in the main chamber. The four-way reducing cross is inserted between the Ti sublimation flange and the turbo pump (see number 8 in Fig. 2). Furthermore, all of the connections, including electrical and cryogenic, are flexible and attached to the bottom of the variable temperature stage to avoid impeding stage movement.

Heating is accomplished by a high-density 150 W heater cartridge (number 1 in Fig. 1). The sample is cooled by flowing chilled nitrogen gas, liquid nitrogen, or a combination of both through the cryogenic block. The cooling medium passes through a

liquid feedthrough (number 8 in Fig. 2), which is connected to 18 in. of 0.25 in. stainless steel bellows using VCR® fittings [Fig. 2(b)]. Welded to the end of the stainless steel bellows is a ±10kV cryogenic break (number 6 in Fig. 1) with 0.125 in. stainless-steel tube. The 0.125 in. stainless-steel tube is bent into a "U" shape and encased in a copper block [Fig. 1(b)], which is attached to the heater block by vented screws. During operation, the sample temperature is monitored by a thermocouple attached to the heater block (see number 3 in Fig. 1). Both the thermocouple and heater power wires are stripped and laced with ceramic beads (see Fig. 1) to minimize vacuum contaminants and prevent arcing. Additionally, the wires are encased in borosilicate glass tubing [Fig. 2(b)] to further prevent arcing before connecting to the electrical feedthrough [number 9 in Fig. 1(a)]. All of the individual components are commercially available except for the heater block and cryogenic assembly.

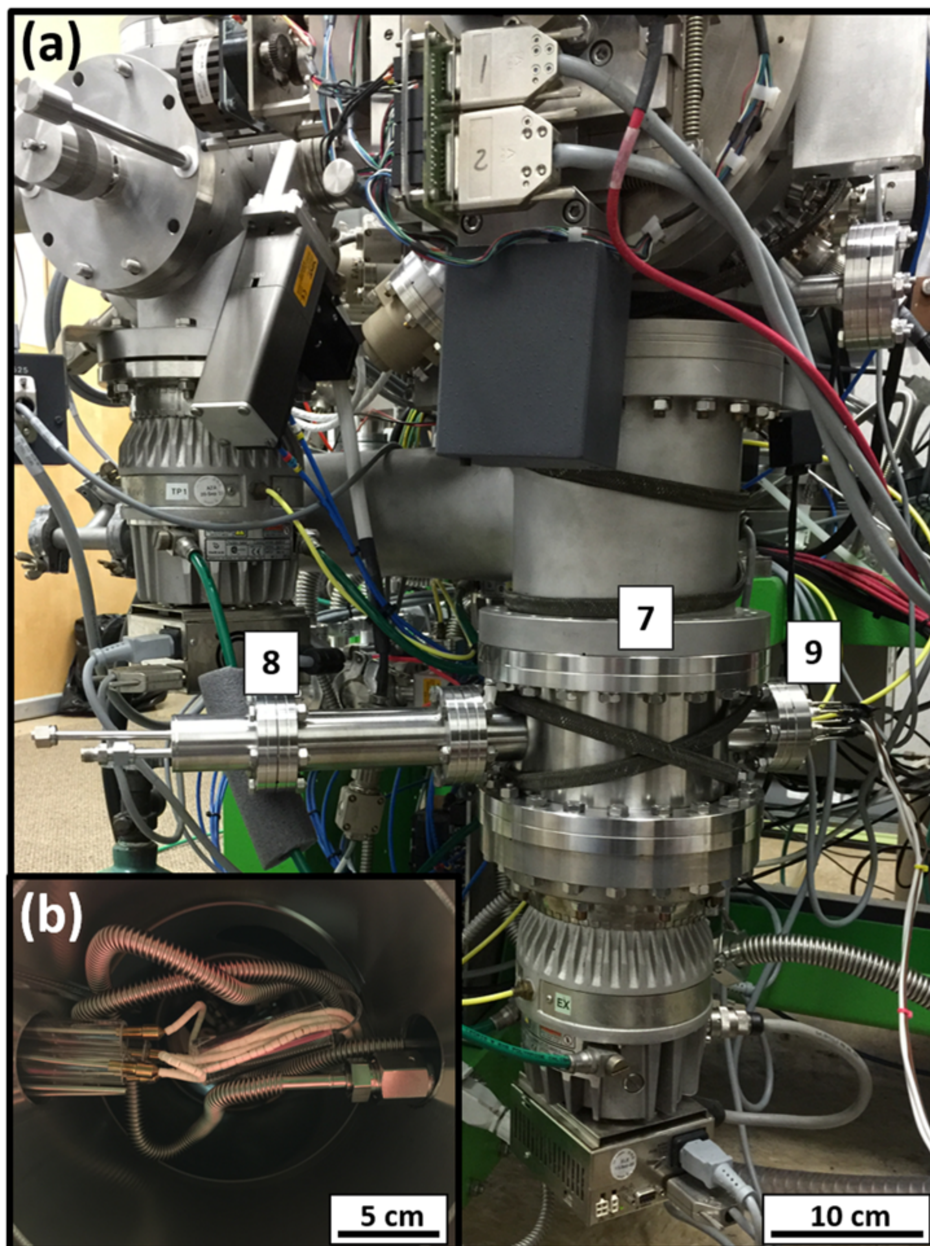

FIG. 2. (Color online) (a) External vacuum connections for the variable temperature stage. (b) Internal electrical and liquid connections—view with the turbo pump removed, looking up at the bottom the variable temperature stage.

4.5.2 Stage electronics

The stage electronics are shown in Fig. 3. The stage electronics float at the sample

bias, typically ±5 kV from ground; therefore, several measures had to be taken to protect the operator from high voltage and to isolate the DC high voltage from the AC line voltage powering the heater and temperature controller. The plexiglass box (number 10 in Fig. 3) serves as an engineering control to protect the operator from high voltage and to house the stage electronics. The isolation transformer (number 12 in Fig. 3) isolates the DC high voltage from the AC line voltage to provide power to the heater and temperature controller. The temperature controller (number 11 in Fig. 3) allows high-accuracy control of the sample temperature. A variable transformer (number 13 in Fig. 3) was incorporated into the stage electronics setup to limit the voltage to the heater. In practical operation, limiting the power to the heater helps prevent the heater filament from shorting and improves the lifetime of the heater. All stage electronic components are simple to set up and are commercially available.

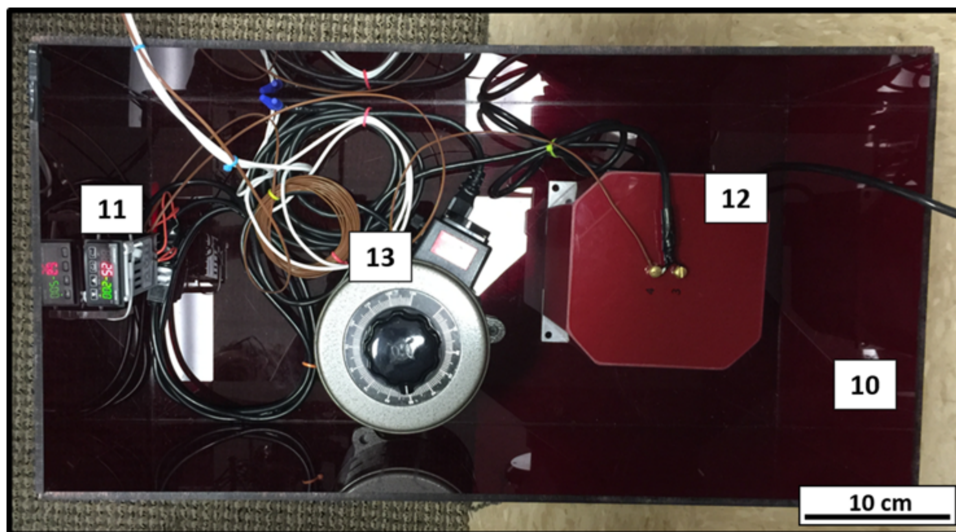

FIG. 3. (Color online) Electronics for the variable temperature stage.

4.5.3 Sample holder

The variable temperature sample holder is shown in Fig. 4 and consists of four oxygen-free, highly conductive copper parts. The first is the sample holder body, which is identical to the Cameca sample holder design in order to be compatible with the sample transfer arm and stage assembly. The second part is the faceplate, which is attached to the sample holder body by four set screws and is interchangeable to accommodate various sample geometries. The faceplate shown in Fig. 4 has a recessed slot window, which is ideal for flat uniform samples (*i.e.*, semiconductor wafer samples) and exhibits an excellent spot-to-spot repeatability. The recessed slot window design has increased mechanical strength and can tolerate thermal stresses compared with the thin Ta faceplate. Third are the copper sample "backs" (blocks), which were machined to fit into the recessed slot window behind the sample [Fig. 4(a)]. They increase thermal uniformity by increasing the thermal contact area on the sample. Finally, the fourth copper part is the back plate, which is used to hold the samples and copper backs in place during analysis. The all-copper design assures the variable temperature sample holder has high thermal conductivity and excellent thermal stabilization characteristics.

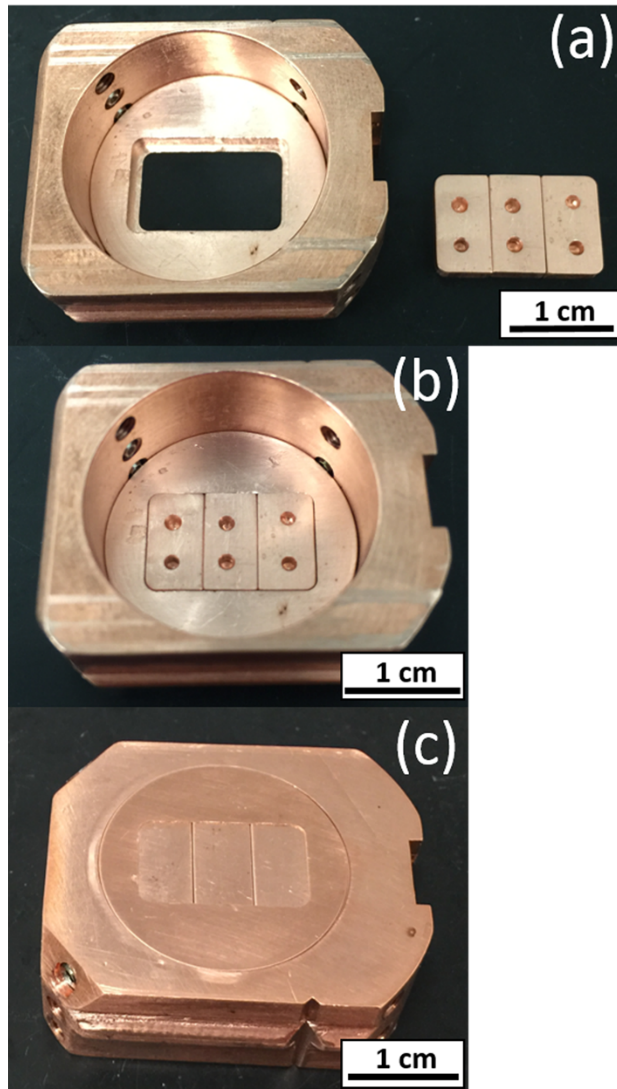

FIG. 4. (Color online) Variable temperature sample holder. (a) Back of sample holder with Cu blocks not inserted. (b) Back of sample holder with Cu blocks inserted. (c) Assembled sample holder.

4.5.4 Operation

Below are the procedures for sample heating and cooling along with sample heating and cooling rates (Fig. 5). The temperature at the sample loading position was measured by mounting a thermocouple in the sample location in the variable temperature sample holder. Under standard operation, the sample temperature is monitored by the

thermocouple located on the variable temperature stage, as shown in Fig. 1. The sample is heated by selecting the desired elevated temperature on the temperature controller and allowing the sample and variable temperature stage to equilibrate. The output power of the heater is limited to 25 W to minimize thermal shock and extend the lifetime of the heater filament. With a 25 W heater output, temperatures ranging from room temperature to 300 °C are obtainable (Fig. 5). Higher elevated temperatures are possible, but to minimize the possibility of damage to the SIMS instrument, temperatures were kept below 400 °C. It is worth noting that the main chamber pressure increases to ~$1x10^{-8}$ Torr at 300 °C.

Sample cooling is accomplished in two steps to minimize thermal shock. First is precooling, achieved by flowing dry nitrogen gas at a rate of 9.5 l/min through 50 ft of 0.25 in. copper tubing submerged in liquid nitrogen until the sample temperature reaches approximately -30 °C. Once the variable temperature stage components and stage assembly are precooled, the second step is to replace the chilled nitrogen gas with liquid nitrogen. Using this procedure, temperatures of -150 °C are routinely achieved. To obtain sample temperatures between -150 °C and room temperature, simultaneous heating and cooling (flowing liquid nitrogen) is used by selecting the desired temperature on the temperature controller. After sample cooling is complete or is no longer required, the liquid nitrogen lines can be disconnected, and the stage assembly can either slowly warm to room temperature or can be rapidly heated to room temperature with the heater.

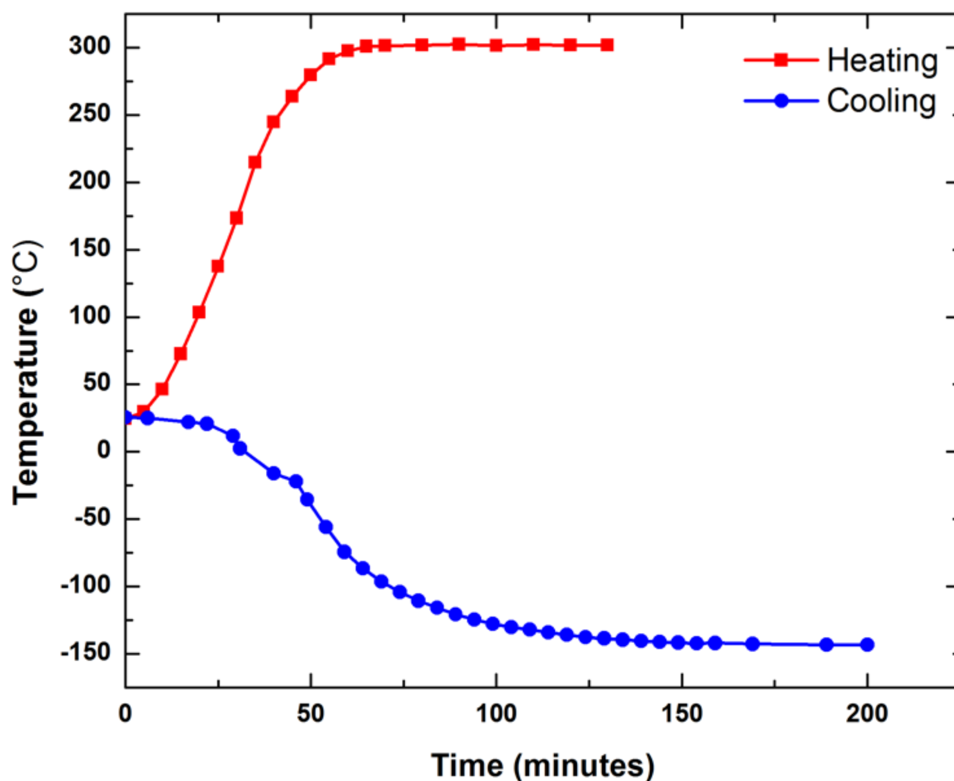

FIG. 5. (Color online) Sample heating and cooling curves. Heating curve (squares) with 25 W output power. Cooling curve (circles) with chilled nitrogen gas (9.5 l/min flow rate) to 30 C then switched to liquid nitrogen.

4.6 Applications

4.6.1 Quickly achieving low background levels of atmospherics in Si

SIMS is commonly used for the detection of atmospherics (H, C, N, and O) in electronic thin films due to its excellent chemical sensitivity (ppm-ppb) and depth profiling capability.[6] However, the amount of time required to perform an atmospheric analysis can be lengthy. The length of time is not specifically due to the analysis, but rather to the time required to minimize atmospheric vacuum contaminants. The traditional atmospheric analysis method consists of: (1) loading the sample into the main

chamber the day prior to the analysis; (2) Ti sublimating over night; and (3) performing the analysis the next day. The traditional method is a multiple-day analysis that requires ~16 h to complete.

In this application, we demonstrate that heating the sample, float zone Si, to 200 °C prior to the atmospheric analysis reduces the time required when compared with the traditional method. The sticking coefficient of vacuum contaminants is reduced at elevated temperatures.[3] By operating at elevated temperatures, the amount of atmospherics absorbed on the sample is reduced, and low atmospheric backgrounds can be quickly achieved. The sample heating procedure consists of: (1) loading the sample into the main chamber; (2) heating the sample to 200 °C for 1 h followed by a 1 h cool-down; and (3) performing the analysis. The heating method required ~2.5 h to perform, making the atmospheric analysis a same-day analysis and improving the analysis time by a factor of six when compared with the traditional method.

Both the traditional and heating method atmospheric analyses were acquired by rastering a 50 nA, -15 keV Cs^+ ion beam at 25 degrees over a 125x125 μm area. A comparison of the measured atmospherics for both analyses is shown in Table I. The atmospheric species, H, C, N, and O, were quantified using relative sensitivity factors from Wilson.[7] Overall, atmospheric background concentrations were reduced using the heating method at a sixth of the time needed for the analysis when compared with the traditional method. Based on these results, sample heating can improve the throughput of the atmospheric analysis if the sample can be heated without adverse effects.

TABLE I. SIMS atmospheric analysis comparison of traditional versus heating method.

	Concentration, atoms/cm^3	
Species	Traditional Method (Room Temperature)	Heating (200° C) Method
H	2.3×10^{17}	1.7×10^{17}
C	1.5×10^{17}	1.3×10^{17}
N	1.1×10^{16}	8.2×10^{15}
O	5.0×10^{17}	3.7×10^{17}

4.6.2 Reduced metastable decay of niobium hydrides

Nb Superconducting Radio Frequency (SRF) cavities are of high interest in the particle accelerator community due to the cost and performance advantages over warm copper.[8] Recently, Grassellino discovered that introducing nitrogen gas during heat treatment doubled or tripled SRF cavity efficiency.[9] Relating the concentration and location of N in the Nb cavity with cavity efficiency is critical to understanding the N enhancement mechanism. The N concentration is presumed to be in the parts-per-million range;[10] therefore, SIMS is ideally suited for this measurement. However, prior to Grassellino's N-doping discovery, Maheshwari[11] observed metastable decay of NbH_n^- ions during the SIMS analysis on nonheat treated Nb. This was due to the high concentration of H in Nb. After heat treatment, the H concentration was reduced, and the NbH_n^- metastable decay was eliminated. During the preliminary SIMS analysis on the N-doped Nb, metastable decay of NbH_n^- was observed and caused a high background around the NbN^- peak [Fig. 6(a)]. High background counts around the NbN^- peak makes the quantification of N difficult, especially for low N concentrations. Heat treatment was proposed, but was not an option in order to preserve the location of N in the sample. The goal is to measure the sample as-is to relate N concentration with SRF cavity

performance.

We measured N in N-doped Nb at cryogenic temperatures (-150 °C) to reduce H mobility and eliminate high background around NbN^- from the metastable decay of NbH_n^-. The experimental SIMS conditions are the same as those in Ref. 11, except a Cameca IMS 7f-GEO equipped with variable temperature stage was used instead of a Cameca IMS 6f. The results from this experiment are shown in Fig. 6. The room temperature Nb mass spectrum [Fig. 6(a)] clearly shows the effect of NbH_n^- metastable decay and high background around the NbN^-. At -150 °C, the Nb mass spectrum [Fig. 6(b)] has a similar shape to the room temperature mass spectrum except the peak-to-background ratio increased by 100x for Nb^- and the metastable decay (high background) around NbN^- was eliminated. Based on the SIMS mass spectrum acquired at -150 °C, cryogenic SIMS is a potential solution to accurately measuring N in N-doped Nb SRF cavities.

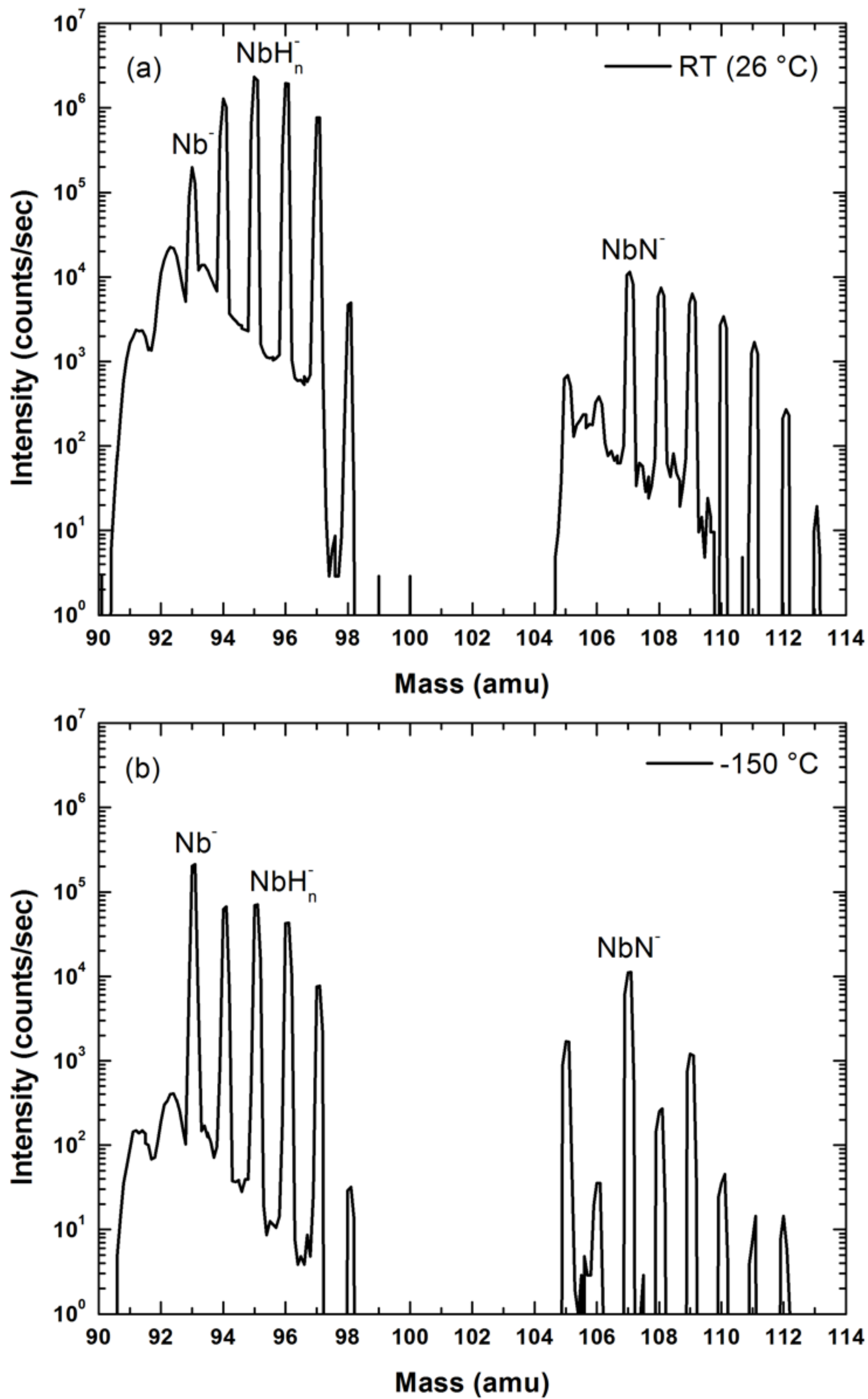

FIG. 6. Nb mass spectra showing the difference in metastable decay between (a) room temperature (26 °C) and (b) -150 °C analysis temperatures.

4.7 Summary and conclusions

We successfully designed and implemented a variable temperature stage for a Cameca IMS 7f-GEO with temperatures ranging from -150 to 300 °C. The variable temperature stage design is innovative and preserves the integrity of the original Cameca design. To minimize the time required to heat and cool the sample, we designed an all-copper variable temperature sampler holder for rapid thermal stability with an interchangeable faceplate for customizability. This variable temperature design requires minimal instrument modification, can be easily adapted to other Cameca SIMS instruments, and costs less than $5000.

We have shown several applications that the variable temperature stage is useful to perform analyses that are not possible at room temperature, such as quickly achieving low atmospheric backgrounds in Si at elevated temperatures and reducing the metastable decay of niobium hydrides at cryogenic temperatures. Our primary application for the variable temperature stage is discussed in detail in Ref. 5.

4.8 Acknowledgements

The authors would like to thank the Institute for Critical Technology and Applied Science and the Nanoscale Characterization and Fabrication Laboratory at Virginia Tech for its support and funding and Darrel Link at the Engineering Science and Mechanics Machine Shop at Virginia Tech for machining parts and design input.

References

[1]M. T. Bernius, S. Chandra, and G. H. Morrison, Rev. Sci. Instrum. **56**, 1347 (1985).

[2]M. Wiedenbeck, D. Rhede, R. Lieckefett, and H. Witzki, Appl. Surf. Sci. 231–232, 888 (2004).

[3]S. M. Hues and P. Williams, J. Vac. Sci. Technol., **A 4**, 1942 (1986).

[4]A. Giordani, J. Tuggle, C. Winkler, and J. Hunter, Surf. Interface Anal. **46**, 31 (2014).

[5]A. Giordani, H. D. Lee, C. Xu, T. Gustafsson, and J. Hunter, "Temperature dependent Cs retention, distribution, and ion yield changes during Cs^+ bombardment SIMS," J. Vac. Sci. Technol., B (submitted).

[6]R. Wilson, F. Stevie, and C. Magee, Secondary Ion Mass Spectrometry: A Practical Handbook for Depth Profiling and Bulk Impurity Analysis (Wiley, New York, 1989).

[7]R. G. Wilson, Int. J. Mass Spectrom. **143**, 43 (1995).

[8]H. Padamsee, RF Superconductivity: Volume II: Science, Technology and Applications (Wiley, American Institute of Physics (AIP), 2009).

[9]A. Grassellino et al., Supercond. Sci. Technol. **26**, 102001 (2013).

[10]M. Kelley and J. Tuggle, personal communication (September 2015).

[11]P. Maheshwari, F. A. Stevie, G. Myeneni, G. Ciovati, J. M. Rigsbee, and D. P. Griffis, AIP Conf. Proc. **1352**, 151 (2011).

5. Temperature Dependent Cs Retention, Distribution, and Ion Yield Changes During Cs^+ Bombardment SIMS

This paper was published in the *Journal of Vacuum Science and Technology B* and reprinted with permission.

5.1 Authors and affiliations

A. Giordani[1,2], H.D. Lee[3], C. Xu[3], T. Gustafsson[3], J. Hunter[1,2,4,a)]

[4] Nanoscale Characterization and Fabrication Laboratory, Virginia Polytechnic Institute and State University, 1991 Kraft Dr., Blacksburg, Virginia 24060

[5] Department of Materials Science and Engineering, Virginia Polytechnic Institute and State University, 445 Old Turner St., Blacksburg, Virginia 24060

[6] Nanophysics Laboratory, Department of Physics and Astronomy, Rutgers University, 136 Frelinghuysen Rd., Piscataway, New Jersey 08854

[7] Materials Science Center, University of Wisconsin-Madison, 1509 University Avenue, Madison, Wisconsin 53706

[a)] Electronic mail: jerry.hunter@wisc.edu

5.2 Abstract

Combining Cs^+ bombardment with positive secondary molecular ion detection (MCs^+) can extend the analysis capability of secondary ion mass spectrometry (SIMS) from the dilute limit (<1 at. %) to matrix elements. The MCs^+ technique has had great success in quantifying the sample composition of III–V semiconductors. However, the MCs^+ has been less effective at reducing the matrix effect for group IV materials, particularly Si-containing compounds. The lack of success in quantifying group IV materials is primarily

attributable to the high Cs surface concentrations overloading the sample surface and lowering ion yields. The Cs overload issue is caused by the mobility and relocation of the implanted Cs to the surface during an analysis. Critical to understanding the material-dependent success of the MCs^+ technique and elucidating the Cs mobility is understanding how Cs is incorporated and distributed into the sample and how the Cs surface concentration affects the ionization processes. The authors provide both new insight for improving the MCs^+ technique by investigating the Cs retention, distribution, and ion yield differences between group III–V and IV materials and a greater understanding of the temperature-dependent mobility and relocation of the implanted Cs. There have been many studies on improving the MCs^+ technique; however, our novel approach to use temperature as a means of controlling the Cs mobility has not been previously explored. Cesium build-up curves were acquired to assess the *in situ* Cs incorporation differences. By utilizing the newly developed variable temperature stage on our SIMS, cesium build-up curves were acquired over a wide range of temperatures (-150 to 300 °C) to show the temperature-dependent relocation of Cs and the effect it has on the ionization processes. Additionally, Cs ionization and neutralization were quantified as a function of Cs fluence and temperature. The Cs retention and distribution differences were determined *ex situ* by measuring the Cs concentration using heat-treatment x-ray photoelectron spectroscopy and heat-treatment medium energy ion scattering. These results allow for a more thorough understanding of the material-dependent success of the MCs^+ technique, the Cs^+-sample interaction, and the temperature component of the Cs mobility.

5.3 Introduction

In secondary ion mass spectrometry (SIMS), cesium and oxygen ions are commonly used as the sputter and analysis beam and are known to enhance secondary ion yields; oxygen enhances positive ion yields; and cesium enhances negative ion yields.[1] The enhancement of secondary ions gives rise to the excellent chemical sensitivity (as low as parts per 10^9 for some materials) of the SIMS technique; however, quantitative SIMS has been limited by matrix effects where secondary ion yields can vary by orders of magnitude depending on the sample composition and the sputtered element. A commonly employed method to minimize SIMS matrix effects requires sputtering with Cs^+ and detecting the positive Cs molecular ions (MCs^+), where M is the dopant, impurity, or matrix element of interest and is known as the MCs^+ technique.[2] This technique expands the analytical range of SIMS well beyond the dilute limit, enabling SIMS to successfully quantify the sample composition of semiconductors as well as the dopants and impurities within. Several studies have shown that the MCs^+ technique has been more effective at reducing matrix effects for III–V[2,3] and less for group IV compounds,[4] particularly Si containing compounds.[5] The material-dependent success of the MCs^+ technique is directly related to the Cs concentration during the analysis,[6] which is proportional to 1/(1 + sputter yield).[7-9] Sputter yield (SY) is the ratio of sputtered atoms to incident ions.

Even though the MCs^+ technique has been heavily studied since the late 1980s,[3,10] more recently,[6,11] the research has focused on elucidating the mobility of the implanted Cs and the effect it has on secondary ion yields, *i.e.*, the MCs^+ formation, for Cs based SIMS analysis. The mobility of implanted atoms in solids is not a new phenomenon, as

Blank *et al.*[12] demonstrated that implanted Xe atoms in Si are mobile, and later, Menzel and Wittmaack[13] confirmed that implanted Cs atoms are mobile in Si. The exact transport mechanism causing Cs to relocate during implantation or bombardment is still unknown;[11] however, the following transport mechanisms have been attributed to the mobility of Cs: thermal diffusion;[14] radiation enhanced diffusion;[15] precipitation;[16] chemical potential; and pressure.[17] The discovery of mobile implanted atoms has lead to a new ion implantation model, the rapid relocation model,[11,18] that accounts for the bulk mobility of the implanted ions and has prompted multiple studies[11,19-24] to gain a better understanding of how the mobile implanted Cs atoms affect the SIMS analysis.

Mobile implanted Cs atoms can have a pronounced effect on the emission of positive secondary ions. This effect is observed and is most prominent during the MCs^+ analysis. Upon Cs^+ bombardment, relocation of the implanted Cs atoms to the receding surface happens nearly instantaneously, causing the surface to overload with Cs. The excess Cs limits the emission of positive secondary ions. Since the success of the MCs^+ technique depends heavily on the Cs^+ emission to form MCs^+, the Cs overload (high Cs concentration) at the surface reduces the emission of Cs^+ to the extent that the MCs^+ fails to eliminate matrix effects. The Cs overload issue is particularly prevalent in low-sputter yield materials (Si and high Si concentration-containing compounds) when compared with high-sputter yield materials (InAs, GaAs, and other group III–V compounds). Several groups[4,23,25-28] have investigated different methods and techniques to circumvent the Cs overload issue and have had some success.

While methods to minimize the Cs overload issue have been developed, the use of temperature as a method to control the relocation of Cs during SIMS analysis has not

been explored. We have built, designed, and implemented a variable temperature stage[29] for a Cameca IMS 7f-GEO, which is rather inexpensive compared to many of other the instrument modifications[25-27] used to remove the Cs overload issue. In this paper, we extend our work on thermal mobility of Cs to alter the surface Cs concentration during a SIMS analysis[23] in several ways. First, we have simplified the heat source by replacing electron bombardment heating from the normal electron gun with a custom designed variable temperature stage. The new variable temperature stage provides a wide temperature range (-150 to 300 °C), uniform temperature distribution, direct measurement of the sample temperature, and precise control over the sample temperature. Second, we expanded the range of tested samples to determine if a trend exists in the temperature-dependent relocation of Cs in III–V and IV semiconductors. Next, we examined the temperature-dependent implanted Cs distribution using high-resolution medium energy ion scattering (MEIS) and x-ray photoelectron spectroscopy (XPS). Then, we quantified the Cs ionization and neutralization as a function of Cs fluence (cesium build-up curves) and temperature during a SIMS analysis. Finally, we calculated the degree of Cs relocation by fitting the cesium build-up curves with the rapid relocation model.[18]

5.4 Experimental

5.4.1 Materials

The following materials were used in this study: Si(100); SiC-4H; Ge(100); InAs(100); GaAs(100); GaSb(100); and, evaporated Au on Si(100). Except for Au on Si, these samples fall into two categories: group IV and III–V elements. Using this set of

samples allowed us to determine if a trend exists in the Cs uptake, distribution, and temperature-dependent relocation between the columns of materials.

5.4.2 Heat-treatment XPS

Postbombardment temperature-dependent Cs concentration measurements were acquired using a PHI Quantera SXM^{TM} XPS equipped with a variable temperature stage (-180 to 250 °C). Cs implantation and sputtering were performed on Cameca IMS-7f Geo SIMS. A 50 nA, 5 keV Cs primary beam at 45 was rastered over a 300 x 300 μm area to form a uniform sputter crater. To insure that all samples were at a steady state Cs concentration, the Cs^{+} or Cs_2^+ secondary ion signals were monitored until the signals were flat. The samples were quickly transferred from the SIMS to the XPS to limit the unavoidable air exposure. Transfer times were less than 1 min. The heat-treatment XPS experiment is detailed in Ref. 23.

5.4.3 Heat-treatment MEIS

Heat-treatment MEIS analyses were performed at Rutgers University using a 400keV ion accelerator and He^{+} ions. The backscattered ions were energy analyzed with a High Voltage Engineering toroidal energy analyzer with a resolution of 200 eV. Depending on the sample, the beam energy was 130 or 190 keV. The spectra were taken at random crystallographic orientations with the incidence direction 7 away from the normal and a total scattering angle of 135 .

The MEIS samples were prepared in a similar manner as the heat-treatment XPS samples, except a 400 nA beam with a 500 x 500 μm raster was stepped across the

sample to implant 10 x 13 mm area. After implantation, samples were quickly (<1min) transferred into a SampleSaver™ and flushed with Ar to minimize air exposure during shipment and prior to the MEIS analysis. Temperature-dependent measurements were obtained in a similar manner to the heat- treatment XPS analyses, but with the ability to measure the Cs concentration with 2 Å resolution depth resolution.

5.4.4 SIMS: cesium build-up curves and sputter yields

Cesium build-up curves are used to study how the secondary ion yields vary as a function of Cs fluence. The Cs of interest for these experiments is from the Cs primary ion beam, which is both the sputter and analysis beam. Cesium build-up curves were acquired with a Cameca IMS-7f Geo equipped with a custom-built variable temperature stage (-150 to 300 °C). A 5 keV Cs^+ primary ion with an incident angle of 45 was used for all measurements. Cesium build-up curves require low Cs primary beam currents. The Cs^+ current used varied from 3 to 6 nA depending on the sample and allowed us to achieve acceptable data density for a 300 x 300 μm crater and a 62 μm analysis area. The following species: Cs^+; Cs_2^+; MCs^+; XCs^+; M^+; and X^+ were investigated for a material to study how the Cs fluence affects the secondary emission. M and X are matrix elements, *i.e.*, InAs: M is In and X is As. All species were sputtered until steady state was achieved as indicated by a flat signal. After the cesium build-up curve is acquired, sputter time is converted to Cs fluence and Cs ionization is calculated (discussed in Sec. III B).

Cs sputter yields were acquired in a similar manner to cesium build-up curves except a 50 nA beam used to sputter a flat bottom crater of sufficient depth to accurately measure with a stylus profilometer. Crater dimensions were measured on a Tencor

Alpha-Step 500 profilometer. Prior to the cesium build-up curves and sputter yield measurements, all samples were cleaned to remove the surface oxide layer and contaminants. Sample cleaning was performed as follows: methanol wipe, followed by a 10-min buffered oxide etch 6:1 bath (ammonium fluoride, hydrofluoric acid), then rinsed in deionized water and dried with N_2 gas, and loaded into the SIMS introduction chamber. In addition to room temperature, cesium build-up curves and sputter yields were acquired at various temperatures ranging from -150 to 300 °C. to assess the temperature dependence. For a detailed description of the variable temperature stage heating and cooling rates, see Ref. 29.

5.5 Modeling and Cs ionization calculation

5.5.1 Modeling Cs retention: rapid relocation model

The rapid relocation model the sputter yield approximation[30] for modeling the retained implanted atoms in a sample. The sputter yield approximation assumes that the implanted atoms are immobile once implanted in the sample and can only migrate to the receding surface passively through sputtering.[11] Therefore, the sputter yield of the material defines the concentration of the implanted atoms.[8,9] However, several studies[12,13,15] have shown that implanted atoms are mobile and that the mobility (active transport) of the implanted atoms needs to be accounted for to accurately model the retained atoms in the sample. The rapid relocation model accounts for the mobility, both active and passive transport, of the implanted atoms to the receding surface. The rapid relocation model redefines the sputter yield as the effective sputter yield (SY_{eff}) by adding an additional parameter, the relocation efficiency (Ψ_{rlc}), to account for the active

transport of the implanted atoms to the sputter yield[11]

$$SY_{eff} \equiv SY + \Psi_{rlc} = \left(1 + \frac{\Psi_{rlc}}{SY}\right). \qquad (1)$$

Therefore, the new effective sputter yield term accounts for both the active (Ψ_{rlc}) and passive (SY) transport of the implanted atoms to the receding surface. The effective sputter yield is simply what the sputter yield would be in the absence of the implanted atoms relocating to the surface. One can model the retained implanted atoms concentration by substituting the effective sputter yield for the sputter yield in the sputter yield approximation.[30] Detailed information on the relocation efficiency and an example of fitting a Cs^+-cesium build-up curve with the rapid relocation model to calculate the relocation efficiency of the implanted Cs atoms in Si can be found in Refs. 11 and 18, respectively.

For this work on the temperature-dependent relocation of Cs in group IV and III–V materials in SIMS, the relocation efficiency is calculated experimentally by fitting the Cs^+-cesium build-up curves with the rapid relocation model. A large relocation efficiency indicates that the implanted Cs atoms are actively transported to the receding surface. Successful modeling of the implanted Cs atoms is critical to understanding the Cs fluence-dependent secondary ion yields changes.

5.5.2 Calculation Cs ionization and neutralization

In this section, we describe a novel method for calculating the Cs ionization and neutralization as a function of Cs fluence. This enables us to assess the degree of

neutralization due to the relocated Cs during Cs^+ bombardment. The underlying assumption for calculating the Cs ionization and neutralization is given in Eq. (2)

$$I_{p(Cs^+)} = \frac{I_{s(Cs^+)}+NL}{\mathrm{T}}, \quad (2)$$

where $I_{p(Cs^+)}$ is that the primary Cs^+ beam current arriving at the sample, $I_{p(Cs^+)}$ is the measured secondary Cs^+ ion current, NL is the neutralization loss, and T is the instrument transmission. Most materials do not have 100% Cs^+ ionization under Cs bombardment;[4] therefore, the other ionized Cs (*i.e.*, Cs^+, Cs_2^+, MCs^+, XCs^+) mass channels, I_s, need to be measured to calculate the total Cs ionization

$$I_{p(Cs^+)} = \frac{[n\times I_{s(Cs_n^+)}+n\times I_{s(MCs_n^+)}+n\times I_{s(MX)}]+NL}{\mathrm{T}}, \quad (3)$$

where n is the number of Cs atoms detected in the mass channel, *i.e.* for Cs^+ n is 1 and for Cs_2^+ n is 2. In order to calculate T, a material with 100% Cs ionization under Cs^+ bombardment is desired as the standard. Au and Pt have 100% Cs ionization because of their high sputter yield and high workfunction.[4,31] For this study, a Au sample (1 μm) thick layer of evaporated Au on Si) was chosen. The procedure for calculating T for Au: (1) Acquire a Cs^+-cesium build-up curve on Au to measure the Cs^+ secondary ion intensity at steady state for a specific Cs bombardment condition (Cs^+ was the only measured ionized Cs mass channel because the other ionized Cs mass channels are negligible compared with the Cs^+ intensity); (2) Convert the measured Cs^+ secondary ion intensity to current by multiplying by the elementary charge ($1.602\mathrm{x}10^{19}$ coulombs); (3) Use Eq. (2) to calculate T with NL being 0 because Au has 100% Cs ionization.

Once T has been determined for a Cs^+ bombardment condition, and if we assume that T is material independent, Cs ionization and neutralization can be calculated for other materials. The procedure for calculating the Cs ionization and neutralization: (1) Acquire the Cs^+, Cs_2^+, MCs^+, XCs^+- cesium build-up curves for a material; (2) Convert the measured steady state secondary ion intensities to current by multiplying by the elementary charge ($1.602x10^{19}$ C); (3) Use Eq. (3) to calculate NL. The result is the total neutralized Cs relative to Au for a material. The ionized Cs is calculated by subtracting the total neutralized Cs from unity. The total calculated ionized Cs is applied to the Cs^+-cesium build-up for a material to show how the Cs ionization varies as a function of Cs fluence. The justification for applying the total Cs ionization to the Cs^+-cesium build-up curve is that Cs^+ is the major channel for ionized Cs.

It is worth noting that T was measured at room temperature, 150, and 300 °C. T was constant at room temperature and 150 °C; however, at 300 °C, the Cs^+ secondary ion yield was reduced due to enhanced Cs relocation at the elevated temperature. Therefore, the room temperature T was used for all Cs ionization and neutralization calculations.

5.6 Results and discussion

5.6.1 *Ex situ* temperature-dependent Cs relocation and distribution

Building on our previous work,[23] the sample set was expanded from Si and InAs to include other group III–V and IV materials, such as SiC, Ge, GaAs, and GaSb, allowing us to better determine if a trend in Cs mobility exists between the two different periodic groups. After the samples were implanted with 5 keV Cs, heat-treatment XPS

was performed to measure the Cs concentration as a function of temperature (see Fig. 1). Before discussing the temperature-dependent trends, it is worth noting the differences in initial room temperature-measured Cs concentration. The measured Cs concentration for the III–V group materials is similar: 2 at. %, compared with 4.5 at. % for group IV materials. The exception to the trend was Ge; however, the result was expected because the retained Cs concentration in the sample depends on the sputter yield of the material.[8,9] The Ge sputter yield is a factor of 2 greater than Si and SiC and much closer to the sputter yield of the III–V materials. Therefore, the measured Cs concentration in Ge should be similar in value to GaAs, InAs, and GaSb, and not to Si or SiC.

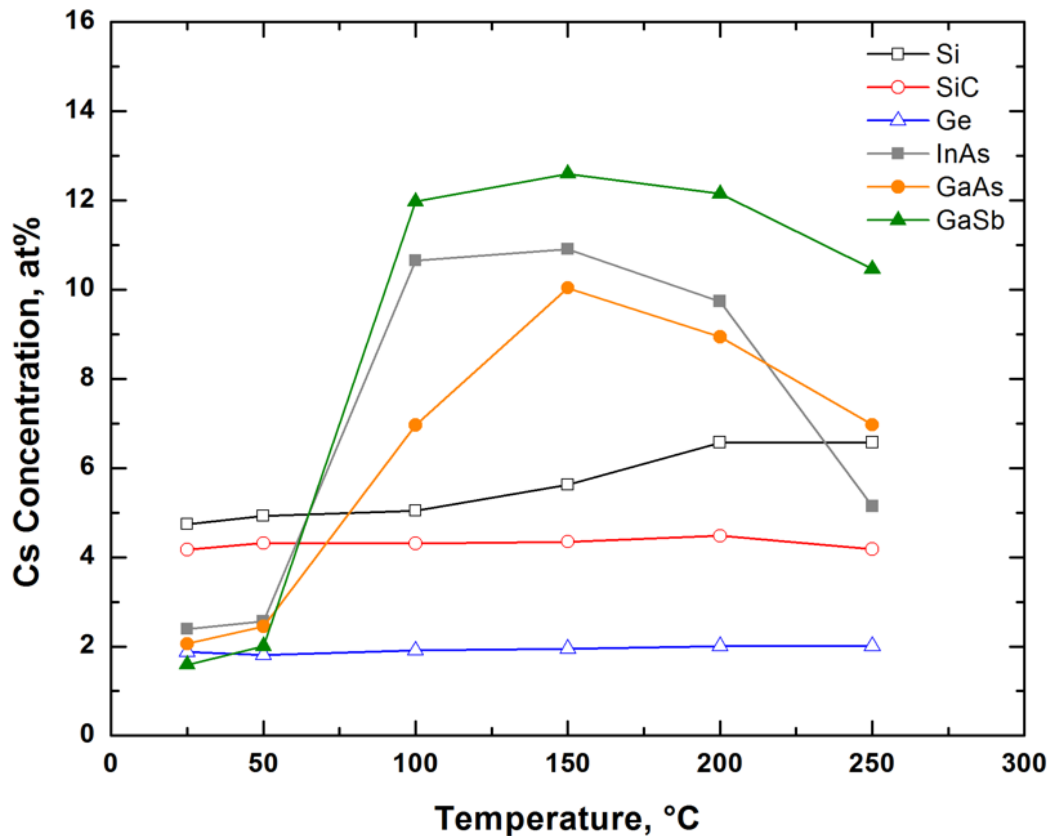

FIG. 1 (Color online) XPS measured Cs concentration as a function of temperature on Si, Ge, SiC, InAs, GaAs, and GaSb. Illustrating the effect sample heating has on the mobility of the implanted Cs between group III-V and IV samples.

Both groups, III–V and IV, exhibit trends in the measured Cs concentration with increasing temperature. The III–V materials had a significant increase in measured Cs concentration between 50 and 100 °C, and at temperatures greater than 150 °C, the Cs concentration began to decrease. In comparison to the III–V materials, the measured Cs concentration for group IV materials remained essentially constant as temperature increased, except for Si, where the measured Cs concentration gradually increased with temperature. In Si, Cs is known to redistribute and form Cs droplets in the presence of minute amounts of oxygen under these Cs bombardment conditions,[32] which could explain the gradual increase in measured Cs concentration compared to the other group IV materials. A possible explanation for the trends between the two groups of materials evident in Fig. 1 is that for group IV materials the implanted Cs relocates to the surface at room temperature. Therefore, the increased temperature has minimal to no effect on the Cs out-diffusion to the surface because it has already occurred at room temperature.

High-resolution MEIS was used to investigate the near- surface Cs distribution postbombardment and temperature-dependent Cs relocation. The room temperature and heat-treatment MEIS spectra of 5 keV Cs implanted in GaAs and Ge are shown in Fig. 2. Both the MEIS and XPS measured Cs concentrations at room temperature are very comparable when comparing similar sample depths. For Ge, the XPS measured Cs concentration at room temperature was 1.9 at. % and for MEIS was 2.4 and 2.1 and 2.3 at. % for GaAs, respectively. The room temperature spectra for both Ge and GaAs show a bimodal distribution of Cs. The narrow peak at 116 keV corresponds to the near-surface Cs, and the broad peak at lower energy corresponds to Cs located within the sample. The

high mobility of the implanted Cs causes the bimodal distribution.[20-23] The exact mechanism for the high mobility of the implanted Cs is not fully understood.[11] The room temperature Ge MEIS spectrum was in agreement with the MEIS results of 5.5 keV Cs implanted in various $Si_{1-x}Ge_x$ samples from Mikami *et al*.[33] and 5 keV Cs implanted in Si from Valizadeh *et al*.[20] The bimodal distribution in the room temperature GaAs MEIS spectrum was contrary to our hypothesis that Cs relocation does not occur in III–V materials based on the heat-treatment XPS results, the Cs^+-cesium build-up curves, and the MCs^+ technique reduces the matrix effect for III–V materials. Two possible explanations for the MEIS bimodal distribution of Cs in GaAs are (1) Cs relocation occurs at room temperature, even though the Cs relocation does not affect the Cs^+ emission in SIMS because the high sputter (10) maintains a low concentration of Cs during the analysis and (2) atmospheric exposure postbombardment during transfer between instruments.

Heat-treatment measurements were performed following the MEIS room temperature measurements, see Fig. 2. Ge was heated to 150 °C for 20 min and GaAs was heated to 200 °C for 35 min prior to the MEIS analysis, and their respective temperature was maintained throughout the analysis. The time and temperatures were chosen based on the heat-treatment XPS results. When heated, the Cs distribution in Ge was relatively unaffected as indicated by small reduction in the near surface Cs peak. However, the Cs distribution in GaAs was significantly affected by temperature, as indicated by the loss of the bimodal distribution and redistribution of Cs toward the surface. Additionally, the higher Cs coverage at elevated temperatures resulted in a downward shift of the substrate signal. This effect can be seen in the As signal in Fig. 2.

Overall, the heat-treatment MEIS results are in agreement with the heat-treatment XPS results, where the group IV materials show a smaller temperature dependence when compared with the III–V materials.

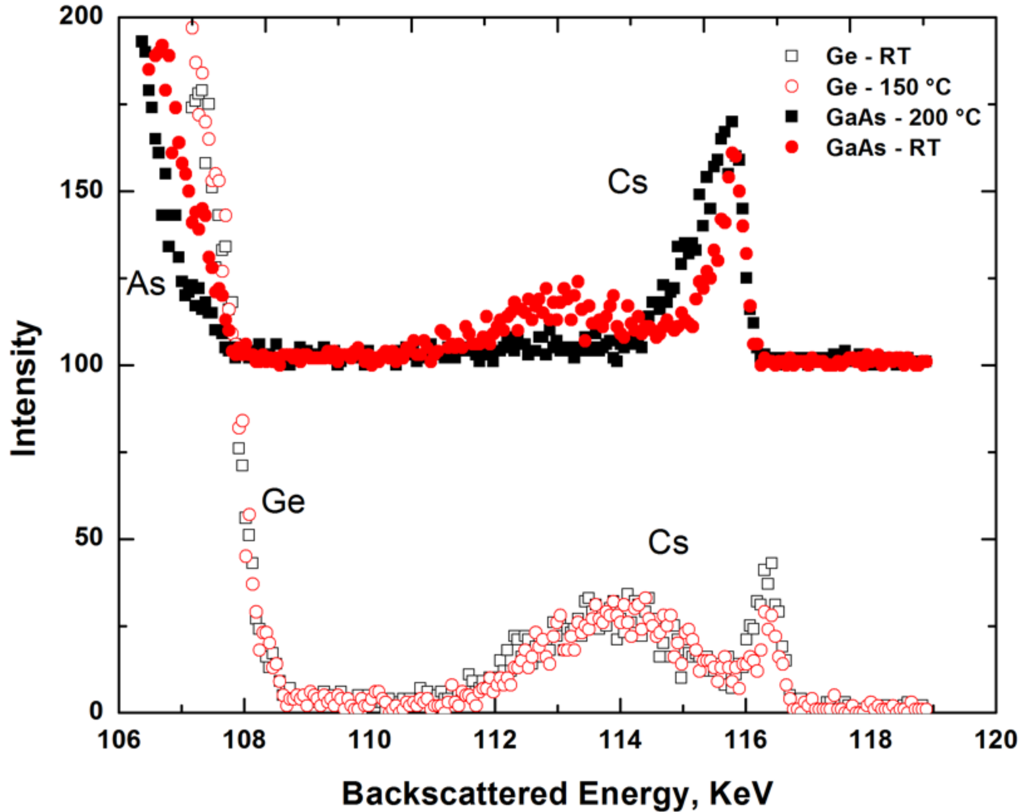

FIG. 2 (Color online) Room temperature (RT) and heat-treatment MEIS spectra of GaAs and Ge after steady state Cs^+ bombardment. The GaAs RT and heat-treatment MEIS spectra were offset by 100, and the data density was reduced by 4x for all spectra for clarity.

Having two independent ex situ characterization techniques (heat-treatment XPS and heat-treatment MEIS) in agreement confirms that there is a temperature-dependent component to the Cs relocation and that temperature can be used as a method to control the relocation of the implanted Cs. In Sec. IV B, we examine the effect that temperature has on the Cs secondary ion emission by performing variable temperature cesium build-

up curves and sputter yield measurements. Our hypothesis, based on this and earlier work,[23] is at elevated temperatures Cs relocation increases causing more of an overload of Cs at the surface, decreasing the Cs ionization and sputter yield. Conversely, at lower temperatures, the Cs relocation will reduce, resulting in an increase of the Cs ionization and sputter yield.

5.6.2 *In situ* temperature-dependent Cs

The *in situ* temperature-dependent Cs ionization section is separated into three subsections for clarity: (1) room temperature, (2) elevated temperatures, and (3) cryogenic temperatures.

5.6.2.1 Room temperature

It is evident from the room temperature Cs^+-cesium build-up curves [Figs. 3(a)–3(e)] that the Cs incorporation, relocation, and ionization (Table I) are sample dependent. The validity of the room temperature measurements were assessed by comparing the Cs_2^+/Cs^+ (R_{21}) ratios (Table I) with the R_{21} ratios at 6 keV at 45 Cs^+ bombardment performed by Wittmaack[4] and are in good agreement. The R_{21} is a metric employed by Wittmaack[4] to obtain the instantaneous Cs coverage, *i.e.*, a larger R_{21} ratio indicates a higher surface Cs concentration.

The different materials are separated into two groups based on the observable trends in the room temperature Cs^+-cesium build-up curves: (1) Si and SiC, and (2) Ge, GaAs, and InAs. Si and SiC exhibit a clear overload and reduction in the ionized Cs as Cs

fluence increases compared to Ge, GaAs, and InAs. For Ge, GaAs, and InAs, the ionized Cs increases and then remains relatively constant as Cs fluence increases. The changes in the ionized Cs in GaAs and InAs are due to changes in topography from Cs bombardment based on the atomic force microscopy (AFM) measurements and not from the relocated Cs affecting the Cs ionization. The trends do not seem related to their group in the periodic table (IV or III–V) but on the sputter yield of the material. A summary of measured sputter yields for the materials is shown in Table I. The approximate factor of two to three differences in sputter yield between Si and SiC and Ge, GaAs, and InAs explains the difference in ionized Cs between the materials.[11] Even though the ionized Cs is relatively large (>90%) for Ge, GaAs, and InAs, Cs relocation still occurs in high-sputter yield materials as well as low-sputter yield materials as shown by the MEIS results in Fig. 2 and Mikami *et al.*[33] The high-sputter yield of the material enables the rapidly relocated Cs to be removed at a sufficient rate to maintain a low Cs surface concentration and, therefore, a high Cs^+ emission. This is not the case in the low sputter yield materials, Si and SiC. The low sputter yield does not remove the relocated Cs at a sufficient rate to maintain a low Cs surface concentration and, as a result, the receding surface becomes overloaded with Cs and the excess Cs limits the emission Cs^+. The reduction in ionized Cs as Cs fluence increases in the sample can be explained by the electron tunneling model.[31] The ionization potential for Cs^+ and the surface work function are competing processes.[34] As the Cs fluence increases in the sample, the incorporated and relocated Cs reduces the surface work function. When the surface work function becomes less than the ionization potential for Cs^+, the ionized Cs is reneutralized, resulting in a decrease in ionized Cs. This effect is most evident in low

sputter yield materials and can be seen in the Si and SiC Cs^+-cesium build-up curves (Fig. 3) at a Cs fluence of $2x10^{15}$ and $1.4x10^{15}$ cm^{-2}, respectively.

We were able to quantify the Cs relocation by fitting the room temperature Cs^+-cesium build-up curves with the rapid relocation model. The Ψ_{rlc} and SY_{eff} values are listed in Table I. It has been established in the literature that Cs is mobile in Si,[13] but this study verifies that Cs is mobile in other materials at room temperature. The Ψ_{rlc} values indicate that Cs has higher mobility in higher sputter yield materials. This may be due to the larger size of atoms in the matrix, allowing Cs to migrate to the surface more easily when compared to smaller atom matrices. By accounting for the relocated Cs with the SY_{eff}, the sputter yield approximation calculated Cs concentrations are closer in agreement with the Cs concentrations measured by XPS and MEIS. These results further reinforce that the implanted Cs is mobile and needs to be accounted when ascertaining the concentration of the implanted Cs in the sample.

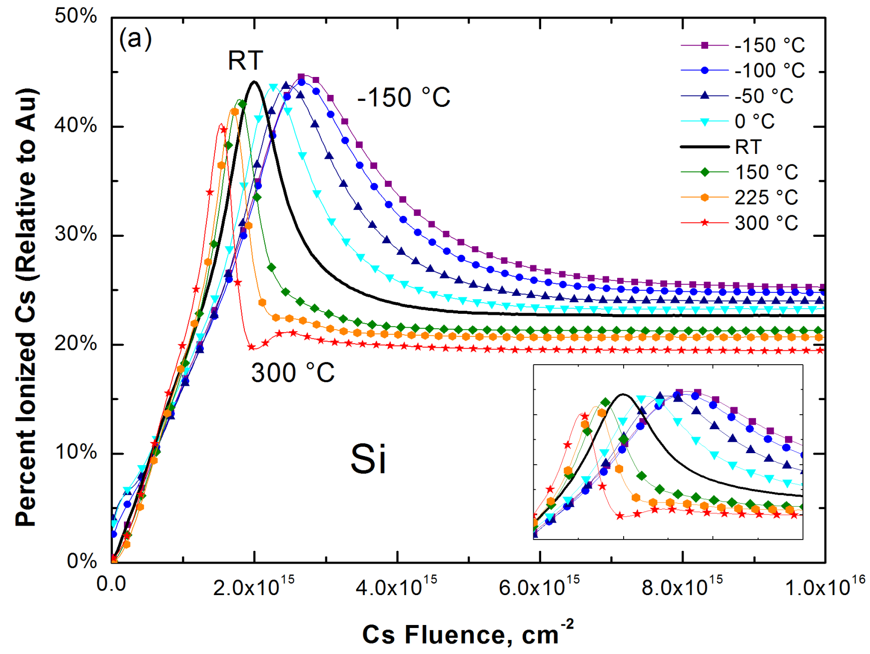
(a)
RT
-150 °C
300 °C
Si
-150 °C
-100 °C
-50 °C
0 °C
RT
150 °C
225 °C
300 °C
Percent Ionized Cs (Relative to Au)
Cs Fluence, cm-2
50%
40%
30%
20%
10%
0%
0.0
2.0x10^15
4.0x10^15
6.0x10^15
8.0x10^15
1.0x10^16

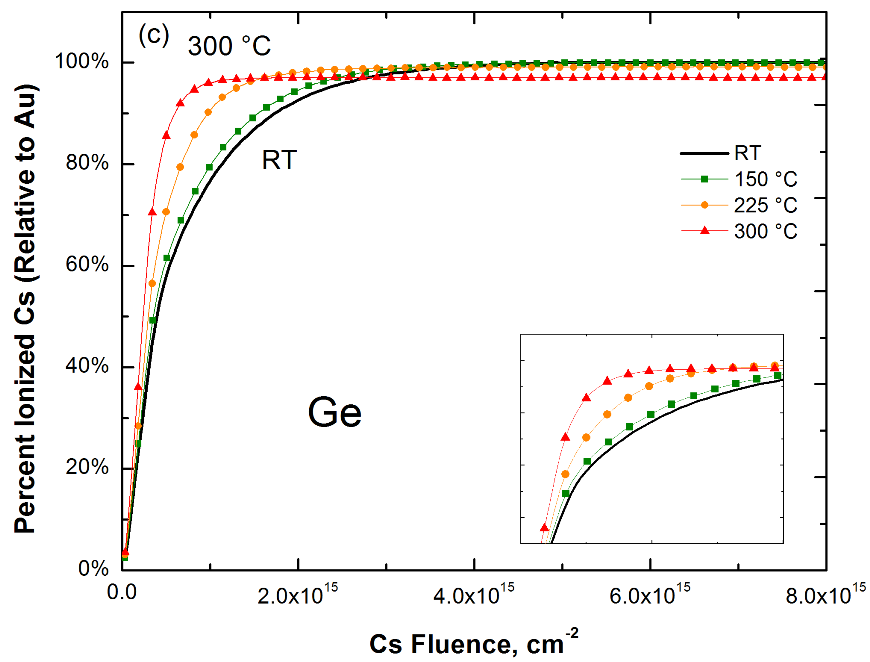
(c)
300 °C
RT
Ge
RT
150 °C
225 °C
300 °C
Percent Ionized Cs (Relative to Au)
Cs Fluence, cm-2
100%
80%
60%
40%
20%
0%
0.0
2.0x10^15
4.0x10^15
6.0x10^15
8.0x10^15

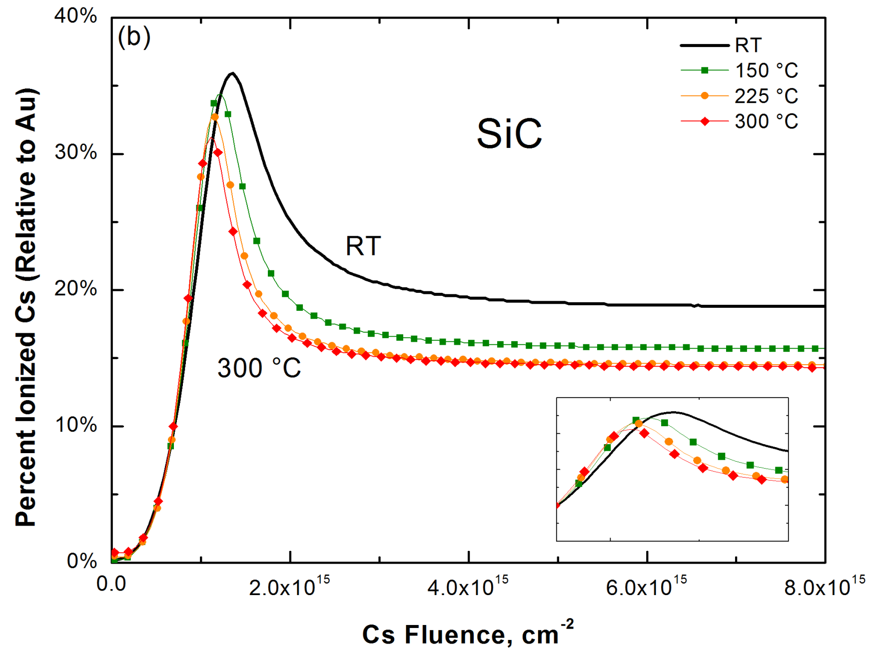

(b)
SiC
RT
300 °C
RT
150 °C
225 °C
300 °C
Percent Ionized Cs (Relative to Au)
Cs Fluence, cm^{-2}
0%
10%
20%
30%
40%
0.0
2.0x10^{15}
4.0x10^{15}
6.0x10^{15}
8.0x10^{15}

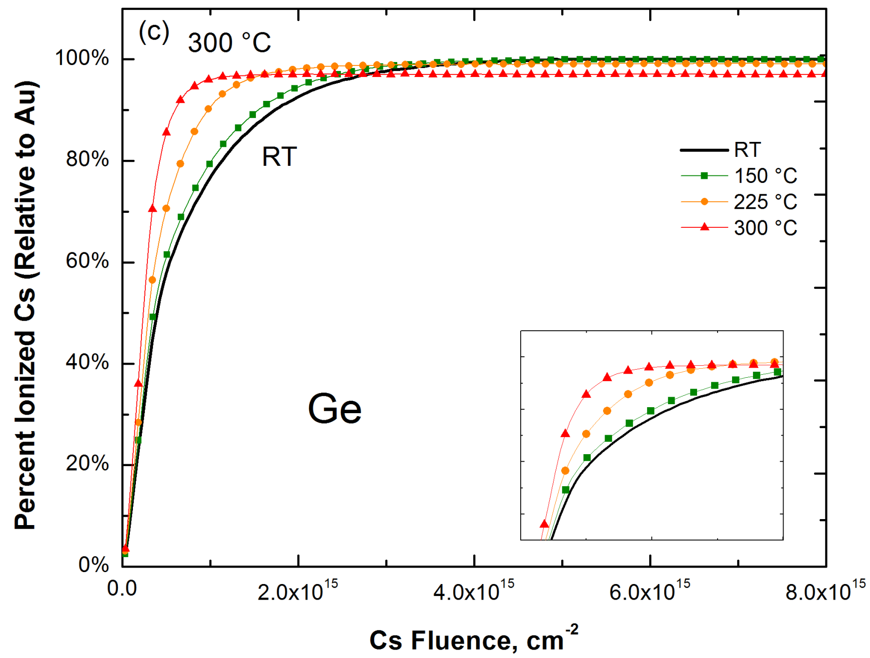

(c)
300 °C
RT
Ge
RT
150 °C
225 °C
300 °C
Percent Ionized Cs (Relative to Au)
Cs Fluence, cm^{-2}
0%
20%
40%
60%
80%
100%
0.0
2.0x10^{15}
4.0x10^{15}
6.0x10^{15}
8.0x10^{15}

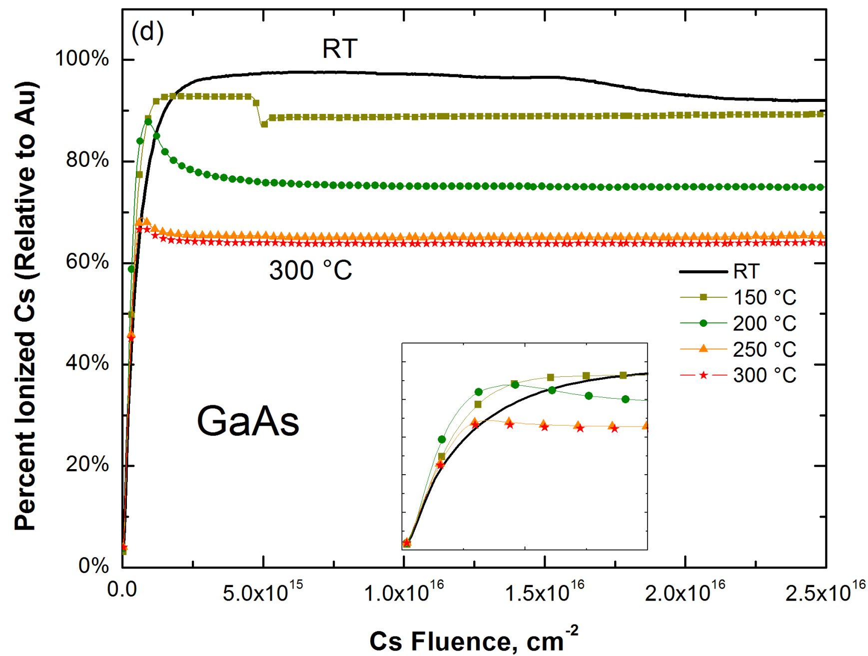

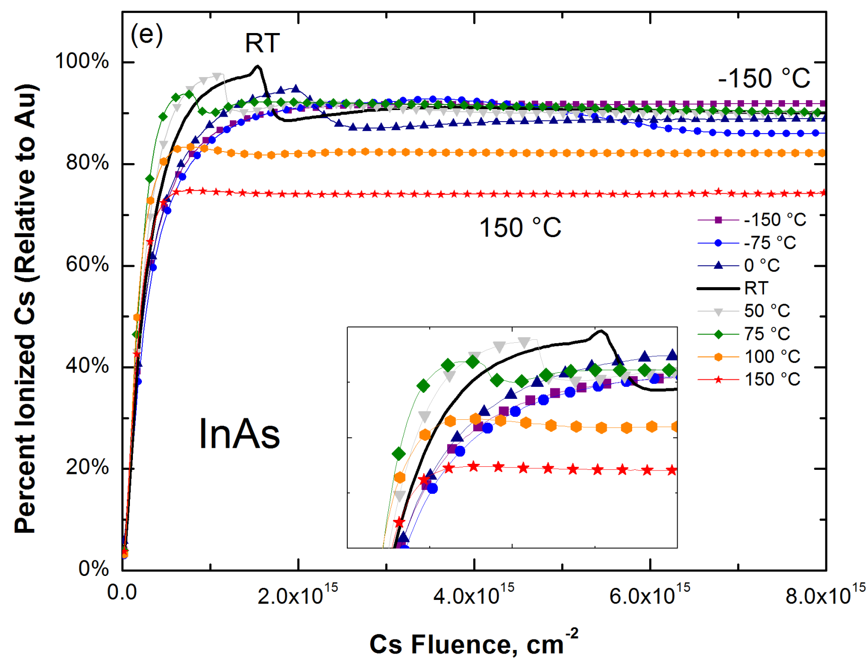

FIG. 3 (Color online) Variable temperture Cs^+-cesium build curves [(a)-(e)] demonstrating the Cs ionization dependence on Cs fluence and temperature. Data density was reduced for clarity. RT is room temperature.

TABLE I. Summary of the measured SY, Ψ_{rlc}, SY_{eff}, R_{21} (Cs_2^+/Cs^+), and steady state Cs ionization as function of temperature for Si, SiC, Ge, GaAs, and InAs. RT is room temperature.

Material	Temperature, °C	Measured SY	Ψ_{rlc}	SY_{eff}	R_{21}	Steady State Cs Ionization (relative to Au)
	-150	5.1 ±0.06	17.9 ±0.06	23.0 ±0.06	$3.1 \times 10^{-2} \pm 7 \times 10^{-5}$	25.3% ±0.2%
Si	RT	4.7 ±0.06	22.1 ±0.06	26.8 ±0.06	$3.4 \times 10^{-2} \pm 1 \times 10^{-4}$	22.7% ±0.2%
	300	4.7 ±0.06	30.0 ±0.06	34.7 ±0.06	$3.6 \times 10^{-2} \pm 1 \times 10^{-4}$	19.4% ±0.2%
	-150	-	-	-	-	-
SiC	RT	4.6 ±0.04	35.4 ±0.04	40.0 ±0.04	$2.9 \times 10^{-2} \pm 4 \times 10^{-4}$	18.8% ±0.1%
	300	4.5 ±0.04	38.5 ±0.04	43.0 ±0.04	$3.3 \times 10^{-2} \pm 2 \times 10^{-4}$	14.2% ±0.1%
	-150	-	-	-	-	-
Ge	RT	8.1 ±0.05	42.8 ±0.05	50.9 ±0.05	$6.9 \times 10^{-3} \pm 2 \times 10^{-5}$	100.0% ±0.4%
	300	8.3 ±0.06	71.1 ±0.05	79.4 ±0.05	$7.5 \times 10^{-3} \pm 4 \times 10^{-5}$	97.0% ±0.4%
	-150	-	-	-	-	-
GaAs	RT	10.2 ±0.06	47.0 ±0.06	57.2 ±0.06	$6.7 \times 10^{-3} \pm 2 \times 10^{-5}$	92.1% ±0.3%
	300	9.7 ±0.06	74.9 ±0.07	84.6 ±0.08	$8.9 \times 10^{-3} \pm 5 \times 10^{-5}$	64.0% ±0.2%
	-150	13.5 ±0.09	74.4 ±0.09	87.9 ±0.09	$6.3 \times 10^{-3} \pm 3 \times 10^{-5}$	91.8% ±0.6%
InAs	RT	13.6 ±0.09	83.1 ±0.09	96.7 ±0.09	$5.6 \times 10^{-3} \pm 3 \times 10^{-4}$	90.4% ±0.8%
	250	12.0 ±0.09	102.4 ±0.09	116.0 ±0.09	$7.8 \times 10^{-3} \pm 5 \times 10^{-5}$	65.0% ±0.2%

5.6.2.2 Elevated temperatures

At elevated temperatures, the Cs relocation is more significant in the III–V materials when compared to the IV materials, as seen in the elevated temperature Cs^+-cesium build-up curves [Figs. 3(a)–3(e)] and in Table I. This result is expected based on the heat-treatment XPS and MEIS results. As the sample temperature increases, the relocation of the implanted Cs to the receding surface increases, which, in turn, increases the reneutralization of the ionized Cs and decreases the ionized Cs. This effect is observed in all of the Cs^+-cesium build-up curves [Figs. 3(a)–3(e)]: as sample temperature increases, ionized Cs decreases. At the maximum elevated temperatures for GaAs and InAs, the ionized Cs decreased by ~35% from room temperature. The decrease in ionized Cs for Si, SiC, and Ge was not as significant, with only ~3%–4% reduction from room temperature at their maximum elevated temperature.

In addition to the steady state ionized Cs decreasing as a function of temperature, other results indicate Cs relocation increased as a function of temperature, such as the changes and trends in the Cs overload peak position, R_{21} ratios, Ψ_{rlc}, SY_{eff}, and SY. As the sample temperature increases, the peak position of the Cs overload occurs at smaller Cs fluences (shallower depths) and the peak Cs ionization decreases, both of which are the result of the increased Cs relocation affecting the rate and amount of Cs ionization at elevated sample temperatures [Figs. 3(a)–3(e)]. The R_{21} ratios increase as a function of temperature for all samples (Table I) indicating that Cs relocation and Cs coverage increases at elevated temperatures. When fitting the elevated temperature Cs^+-cesium build-up curves with the rapid relocation model, the Ψ_{rlc} increased with increasing sample temperature for all materials, signifying that the active transport of the implanted

Cs increased as a function of temperature. An increase in the Ψ_{rlc} will result in an increase in the SY_{eff} as the sample temperature rises due to the SY_{eff} dependence on the Ψ_{rlc} [Eq. (1)]. As shown in Table I, the measured SY decreased as sample temperature increased for some materials, particularly the III–V materials. We postulate this is due to the increased sputtering of the relocated Cs atoms versus the matrix atoms based on the SY dependence with electron gun current from our previous work.[23] Yet, the work of MacLaren[35] indicated that GaAs undergoes a phase change from amorphous to crystalline at the surface at 100 °C under Cs^+ bombardment due to the annealing temperature. Therefore, the observed changes in SY could be due to a change in crystallinity and not from sputtering of more of the relocated Cs. Although we did not examine the crystal structure, an experiment to correlate crystallinity changes with sample temperature under Cs^+ bombardment would be worthwhile.

5.6.2.3 Cryogenic temperatures

In situ cryogenic measurements were performed on Si and InAs, and the results are shown in Figs. 3(a) and 3(e) and in Table I. Based on the trends from the elevated temperatures Cs^+-cesium build-up curves, we chose Si to represent the Cs overload IV materials and InAs to represent the non-Cs overload III–V materials. At cryogenic sample temperatures, we hypothesized that Cs relocation would decrease resulting in an increase in the steady state Cs ionization, produce Cs^+ ion yields that are conducive for the MCs^+ technique, and alleviate matrix effects. In the simple single element matrix of Si, the trends in the cryogenic Cs^+-cesium build-up curves were as hypothesized; however, in the more complicated binary matrix of InAs, other factors that were

unexpected affected the Cs ionization. At -150 °C, the steady state Cs ionization increased ~3% from room temperature for Si and ~1% for InAs. In Si, as the sample temperature decreased, the Cs ionization peak occurred at larger Cs fluences (deeper in the sample), requiring more Cs to cause the Cs overload in the sample. This result is indicative of a reduction in Cs relocation at cryogenic temperatures. This trend was as expected; however, ideally, the Cs overload peak would have been eliminated at -150 °C. The trend in the R_{21} ratios for Si also confirms that the Cs relocation and coverage has decreased with decreasing sample temperatures. For both Si and InAs, the Ψ_{rlc} and SY_{eff} decreased as temperature decreased, demonstrating that the active transport of the implanted Cs has decreased. The measured sputter yield for Si increased with decreasing temperature as shown in Table I. The increase in sputter yield for Si at colder temperatures agrees with our original hypothesis that at cryogenic temperatures, the lower Cs surface concentration allows for more of the matrix atoms to be removed versus sputtering of the primary beam implanted Cs atoms.

Comparing the InAs -150 °C with the room-temperature Cs^+-cesium build-up curve, the obvious difference between the two is the disappearance of the fluctuations in the Cs ionization in the -150 °C Cs^+-cesium build-up curve. The fluctuations in the Cs ionization in the room-temperature Cs^+-cesium build-up curve were due to changes in the sample topography from Cs^+ bombardment. AFM was performed on both the room temperature and -150 °C at steady state (Cs fluence of $8x10^{15}$ cm^{-2}) to determine if there were any differences in surface topography. The average roughness for the room temperature and -150 °C were 10.1±0.6 Å and 5.6±0.3 Å, respectively. The approximate factor of 2 difference in roughness could be attributed to the reduction Cs mobility at

cryogenic temperatures or to the fact that sputter-induced topography is reduced at cryogenic temperatures. Nevertheless, operating at cryogenic temperatures could be beneficial for depth profiles when depth resolution is of concern. The sputter induced topography begins to reappear at 75 and 0 °C, causing fluctuations in the ionized Cs and affecting the steady state Cs ionization [Fig. 3(e)]. Due to the sputter-induced topography, neither the R_{21} ratios nor the measured sputter yield decrease as temperature decreases. Additional experiments are needed to obtain a better understanding of the Cs^+-InAs interaction at intermediate temperatures between room temperature and -150 °C.

5.7 Summary and conclusions

Several *in situ* (cesium build-up curves) and *ex situ* (XPS and MEIS) characterization techniques were combined with the rapid relocation model to expand the knowledge of the fundamental behavior of the implanted Cs in materials other than Si. To assess the degree of Cs neutralization during Cs^+ bombardment, we developed a novel method for quantifying the total Cs ionization by accounting for the major channels that ionized Cs could form: Cs^+, Cs_2^+, MCs^+, and XCs^+. Cs relocation is prevalent in all the materials that were examined; however, the steady state Cs ionization is affected the most by the relocated Cs in low sputter yield materials (Si and SiC) compared to high sputter yield materials (Ge, GaAs, and InAs). These results explain why the MCs^+ technique does not reduce the matrix effect in low sputter yield materials and reduces the matrix effect for high sputter yield materials.

The primary focus of this work was to determine if a temperature-dependent

component to the Cs relocation exists and, if so, whether it is possible to take advantage of that aspect to produce Cs^+ ion yields that are conducive for the MCs^+ technique. We have demonstrated a temperature-dependent component to the Cs relocation through *ex situ* heat-treatment XPS and MEIS and *in situ* variable temperature cesium build-up curves. At elevated temperatures, the Cs relocation is enhanced, and the steady state Cs^+ ionization decreased for all the materials examined. At cryogenic temperatures, the Cs relocation is reduced, and the steady state Cs^+ ionization increased for Si and InAs. In the case of InAs, the steady state Cs^+ ionization at intermediate temperatures between room temperature and -150 °C was affected by the sputter-induced topography from the Cs^+ ion beam.

The question still remains: is operating at cryogenic sample temperatures a potential solution to the Cs overload? The trend in the Cs^+-cesium build-up curves for Si as sample temperature decreases indicates that Cs relocation is reduced but not eliminated, even at -150 °C. This indicates that other forces may be causing the implanted Cs to relocate, such as a radiation enhanced diffusion,[15] precipitation,[16] chemical potential, and/or pressure.[17]

5.8 Acknowledgments

The authors would like to thank the Institute for Critical Technology and Applied Science and the Nanoscale Characterization and Fabrication Laboratory at Virginia Tech for support and funding. A special thanks to Dr. Klaus Wittmaack for all the insightful discussions on Cs^+ based SIMS and the rapid relocation model.

References

[1]C. A. Anderson, Int. J. Mass Spectrom. Ion Phys. 2, 61 (1969).

[2]Y. Gao, Surf. Interface Anal. 14, 552 (1989).

[3]C. Magee, W. Harrington, and E. Botnick, Int. J. Mass Spectrom. 103, 45 (1990).

[4]K. Wittmaack, Nucl. Instrum. Methods B 85, 374 (1994).

[5]H. E. Smith, B. H. Tsao, and J. D. Scofield, Mater. Sci. Forum 527–529, 629 (2006).

[6]K. Wittmaack, Surf. Sci. 606, L18 (2012).

[7]H. Liebl, J. Vac. Sci. Technol. 12, 385 (1975).

[8]V. R. Deline, C. A. Evans, and P. Williams, Appl. Phys. Lett. 33, 578 (1978).

[9]V. R. Deline and W. Katz, Appl. Phys. Lett. 33, 832 (1978).

[10]Y. Gao, J. Appl. Phys. 64, 3760 (1988).

[11]K. Wittmaack, Surf. Sci. Rep. 68, 108 (2013).

[12]P. Blank, K. Wittmaack, and F. Schulz, Nucl. Instrum. Methods 132, 387 (1976).

[13]N. Menzel and K. Wittmaack, Nucl. Instrum. Methods 191, 235 (1981).

[14]A. Pargellis and M. Seidl, J. Vac. Sci. Technol., A 1, 1388 (1983).

[15]K. Wittmaack and P. Blank, Appl. Phys. Lett. 31, 21 (1977).

[16]E. W. Thomas and D. McPhail, Nucl. Instrum. Methods B 90, 482 (1994).

[17]A. Mutzke and W. Eckstein, Nucl. Instrum. Methods B 266, 872 (2008).

[18]K. Wittmaack, Nucl. Instrum. Methods B 267, 2846 (2009).

[19]K. Wittmaack, Int. J. Mass Spectrom. 313, 68 (2012).

[20]R. Valizadeh, J. A. van den Berg, R. Badheka, A. Al Bayati, and D. G. Armour, Nucl. Instrum. Methods B 64, 609 (1992).

[21]P. Philipp, T. Wirtz, H.-N. Migeon, and H. Scherrer, Int. J. Mass Spectrom. 264, 70

(2007).

[22]P. Philipp, P. Barry, and T. Wirtz, Surf. Interface Anal. 46, 7 (2014).

[23]A. Giordani, J. Tuggle, C. Winkler, and J. Hunter, Surf. Interface Anal. 46, 31 (2014).

[24]L. Houssiau, C. Noel, N. Mine, K. W. Jung, W. J. Min, and D. W. Moon, Surf. Interface Anal. 46, 22 (2014).

[25]T. Wirtz and H.-N. Migeon, Appl. Surf. Sci. 231–232, 940 (2004).

[26]J. Brison and L. Houssiau, Nucl. Instrum. Methods B 259, 984 (2007).

[27]R. Pureti, B. Douhard, D. Joris, A. Merkulov, and W. Vandervorst, Surf. Interface Anal. 46, 25 (2014).

[28]B. Berghmans, J. Rip, and W. Vandervorst, Surf. Interface Anal. 43, 225 (2011).

[29]A. Giordani, J. Tuggle, and J. L. Hunter, Jr., J. Vac. Sci. Technol. B 34, 03H112 (2016).

[30]F. Schulz and K. Wittmaack, Radiat. Eff. 29, 31 (1976).

[31]M. L. Yu and N. D. Lang, Phys. Rev. Lett. 50, 127 (1983).

[32]A. Giordani, J. Tuggle, C. Winkler, and J. Hunter, J. Surf. Interface Anal. 46, 43 (2014).

[33]A. Mikami, T. Okazawa, and Y. Kido, Jpn. J. Appl. Phys. 47, 2234 (2008).

[34]E. Niehuis, T. Grehl, F. Kollmer, R. Moellers, D. Rading, R. Kersting, and B. Hagenhoff, Surf. Interface Anal. 43, 204 (2011).

[35]S. W. MacLaren, J. Vac. Sci. Technol., A 10, 468 (1992).

6. Summary and Conclusions

This dissertation encompasses multiple projects that study the Cs^+-sample interaction in an effort to gain a better understanding of how the implanted Cs affects the MCs^+ analysis. It also investigated the temperature-dependent component of the Cs mobility.

The first project examined the evolution of Cs droplets in the Si crater bottom post Cs^+ bombardment. This study confirmed that the implanted Cs is mobile within the SIMS crater and that Cs droplets form when exposed to oxygen (O_2 or atmosphere). The Cs droplets evolved as a function of oxygen (O_2 or atmosphere) exposure and go through a series of different morphologies before arriving in their final form. It was also concluded that Cs droplets are affected by heat, either from the electron beam in the SEM or by conduction heating on a vacuum hot stage. The second project investigated elevated temperatures, both *ex situ* and *in situ*, as a potential method to change the location and concentration of Cs in the sample. For *in situ* heating, electron bombardment heating while simultaneously sputtering with Cs was examined as method for altering the Cs concentration during the SIMS analysis. The intent was to lower the instantaneous Cs concentration to produce ion yields that are favorable for the MCs^+ technique. However, *in situ* heating with the Normal-incidence Electron Gun (NEG) proved to be an unsuccessful method for lowering the instantaneous Cs concentration and, as a result, did not produce Cs^+ secondary ion yields that were conducive for the MCs^+ technique. Additionally, several issues with characterizing the implanted Cs were discussed, especially with electron-based techniques. XPS was proven to be a more reliable method for quantifying the surface Cs concentration versus the other techniques studied. *Ex situ* heating confirmed that more implanted Cs was retained in InAs than Si. The results from this study clearly indicate a material-based difference in the amount of incorporated Cs, which could be the defining reason why the MCs^+ technique reduces the matrix for some materials and not for others. The third project builds upon the results from the second project: that temperature can be used as a method to control the instantaneous Cs

concentration during the SIMS analysis. We designed and implemented a variable temperature stage for our Cameca IMS 7f-GEO with temperatures ranging from -150 °C to 300 °C. This enabled us to perform *in situ* variable temperature measurements to study the temperature-dependent relocation of the implanted Cs. The fourth project investigated the temperature-dependent Cs relocation, uptake, and distribution in group III-V and V materials. A temperature-dependent component of the Cs relocation was confirmed by *ex situ* heat-treatment XPS and MEIS and *in situ* variable temperature cesium build-up curves. At elevated temperatures, the Cs relocation was enhanced and the steady state Cs^+ ionization decreased, and at cryogenic temperatures, the Cs relocation was reduced and the steady state Cs^+ ionization increased. In addition, a novel method was developed for quantifying the total Cs ionization and neutralization. The trend in the Cs^+-cesium build-up curves for Si as sample temperature decreases indicates that Cs relocation is reduced but not eliminated, even at -150 °C. This indicates that other forces may be causing the implanted Cs to relocate.

Appendix: Copyright Permission Letters

JOHN WILEY AND SONS LICENSE
TERMS AND CONDITIONS

Feb 12, 2016

This Agreement between Andrew J Giordani ("You") and John Wiley and Sons ("John Wiley and Sons") consists of your license details and the terms and conditions provided by John Wiley and Sons and Copyright Clearance Center.

License Number	3806540974374
License date	Feb 12, 2016
Licensed Content Publisher	John Wiley and Sons
Licensed Content Publication	Surface & Interface Analysis
Licensed Content Title	On the evolution of Cs droplets in SIMS craters
Licensed Content Author	Andrew Giordani,Jay Tuggle,Christopher Winkler,Jerry Hunter
Licensed Content Date	Oct 27, 2014
Pages	3
Type of use	Dissertation/Thesis
Requestor type	Author of this Wiley article
Format	Print and electronic
Portion	Full article
Will you be translating?	No
Title of your thesis / dissertation	A Fundamental Study on the Relocation, Uptake, and Distribution of the Cs+ Primary Ion Beam During the Secondary Ion Mass Spectrometry Analysis
Expected completion date	Mar 2016
Expected size (number of pages)	100
Requestor Location	Andrew J Giordani 1991 Kraft Drive BLACKSBURG, VA 24060 United States Attn: Andrew J Giordani
Billing Type	Invoice
Billing Address	Andrew J Giordani 1991 Kraft Drive BLACKSBURG, VA 24060 United States Attn: Andrew J Giordani

JOHN WILEY AND SONS LICENSE
TERMS AND CONDITIONS

Feb 12, 2016

This Agreement between Andrew J Giordani ("You") and John Wiley and Sons ("John Wiley and Sons") consists of your license details and the terms and conditions provided by John Wiley and Sons and Copyright Clearance Center.

License Number	3806540803095
License date	Feb 12, 2016
Licensed Content Publisher	John Wiley and Sons
Licensed Content Publication	Surface & Interface Analysis
Licensed Content Title	Temperature dependent relocation of the cesium primary ion beam during SIMS analysis
Licensed Content Author	Andrew Giordani,Jay Tuggle,Christopher Winkler,Jerry Hunter
Licensed Content Date	Aug 7, 2014
Pages	4
Type of use	Dissertation/Thesis
Requestor type	Author of this Wiley article
Format	Print and electronic
Portion	Full article
Will you be translating?	No
Title of your thesis / dissertation	A Fundamental Study on the Relocation, Uptake, and Distribution of the Cs+ Primary Ion Beam During the Secondary Ion Mass Spectrometry Analysis
Expected completion date	Mar 2016
Expected size (number of pages)	100
Requestor Location	Andrew J Giordani 1991 Kraft Drive BLACKSBURG, VA 24060 United States Attn: Andrew J Giordani
Billing Type	Invoice
Billing Address	Andrew J Giordani 1991 Kraft Drive BLACKSBURG, VA 24060 United States

AIP PUBLISHING LLC LICENSE TERMS AND CONDITIONS

Feb 19, 2016

All payments must be made in full to CCC. For payment instructions, please see information listed at the bottom of this form.

License Number	3806560224647
Order Date	Feb 12, 2016
Publisher	AIP Publishing LLC
Publication	Journal of Vacuum Science & Technology B
Article Title	Design and implementation of a custom built variable temperature stage for a secondary ion mass spectrometer
Author	Andrew Giordani,Jay Tuggle,Jerry L. Hunter Jr.
Online Publication Date	Feb 12, 2016
Volume number	34
Issue number	3
Type of Use	Thesis/Dissertation
Requestor type	Author (original article)
Format	Print and electronic
Portion	Excerpt (> 800 words)
Will you be translating?	No
Title of your thesis / dissertation	A Fundamental Study on the Relocation, Uptake, and Distribution of the Cs+ Primary Ion Beam During the Secondary Ion Mass Spectrometry Analysis
Expected completion date	Mar 2016
Estimated size (number of pages)	100
Total	**0.00 USD**

Terms and Conditions

American Vacuum Society -- Terms and Conditions: Permissions Uses

American Vacuum Society ("AVS") hereby grants to you the non-exclusive right and license to use and/or distribute the Material according to the use specified in your order, on a one-time basis, for the specified term, with a maximum distribution equal to the number that you have ordered. Any links or other content accompanying the Material are not the subject of this license.

1. You agree to include the following copyright and permission notice with the reproduction of the Material:"Reprinted with permission from [FULL CITATION]. Copyright [PUBLICATION YEAR], American Vacuum Society." For an article, the copyright and permission notice must be printed on the first page of the article or book chapter. For photographs, covers, or tables, the copyright and permission notice may appear with the Material, in a footnote, or in the reference list.
2. If you have licensed reuse of a figure, photograph, cover, or table, it is your responsibility to ensure that the material is original to AVS and does not contain the copyright of another entity, and that the copyright notice of the figure, photograph, cover, or table does not indicate that it was reprinted by AVS, with permission, from another source. Under no circumstances does AVS, purport or intend to grant permission to reuse material to which it does not hold copyright.
3. You may not alter or modify the Material in any manner. You may translate the Material into another language only if you have licensed translation rights. You may not use the Material for promotional purposes. AVS reserves all rights not specifically granted herein.
4. The foregoing license shall not take effect unless and until AVS or its agent, Copyright Clearance Center, receives the Payment in accordance with Copyright Clearance Center Billing and Payment Terms and Conditions, which are

AIP PUBLISHING LLC LICENSE
TERMS AND CONDITIONS

Mar 17, 2016

This Agreement between Andrew J Giordani ("You") and AIP Publishing LLC ("AIP Publishing LLC") consists of your license details and the terms and conditions provided by AIP Publishing LLC and Copyright Clearance Center.

License Number	3831510737921
License date	Mar 17, 2016
Licensed Content Publisher	AIP Publishing LLC
Licensed Content Publication	Journal of Vacuum Science & Technology B
Licensed Content Title	Temperature dependent Cs retention, distribution, and ion yield changes during Cs+ bombardment SIMS
Licensed Content Author	Andrew Giordani,Hang Dong Lee,Can Xu, et al.
Licensed Content Date	Mar 14, 2016
Licensed Content Volume Number	34
Licensed Content Issue Number	3
Type of Use	Thesis/Dissertation
Requestor type	Author (original article)
Format	Print and electronic
Portion	Excerpt (> 800 words)
Will you be translating?	No
Title of your thesis / dissertation	A Fundamental Study on the Relocation, Uptake, and Distribution of the Cs+ Primary Ion Beam During the Secondary Ion Mass Spectrometry Analysis
Expected completion date	Mar 2016
Estimated size (number of pages)	100
Requestor Location	Andrew J Giordani 1991 Kraft Drive BLACKSBURG, VA 24060 United States Attn: Andrew J Giordani
Billing Type	Invoice
Billing Address	Andrew J Giordani 1991 Kraft Drive